Heat transfer in the finned fluidized bed tubular heat exchanger
by Joon Taik Kim

A thesis submitted to the Graduate Faculty in partial fulfillment of the requirements for the degree of MASTER OF SCIENCE in Chemical Engineering
Montana State University
© Copyright by Joon Taik Kim (1970)

Abstract:
Local and average heat transfer coefficients for bed -to-wall heat transfer from a fluidized bed tubular heat exchanger with extended surfaces were investigated.

The fluidized bed tubular heat exchanger consisted of a 44-inch long, 5.5-inch inside diameter shell with 19, 3/4-inch diameter stainless steel tubes arranged in a 1-inch triangular pitch. Air was used as the fluidizing medium and glass spheres of 0.0185-inch average diameter were used in this study.

Tubes at the four possible tube locations tube were heated electrically. 3/16-inch stainless steel wire was used as an extended surface. The stainless steel wire was wrapped around the outside of each 19 tubes in a helical sprial. Variables studied include particle concentration, gas mass velocity and twist ratio.

The Results of This Study Are as Follows 1. Gradual increase in the weighted average heat transfer coefficients with respect to the number extended surface were observed. Local heat transfer coefficients decreased with the distance from the entrance of the fluidized bed. Tube locations had only a slight effect on local heat transfer coefficients.

2. The average sectional coefficients according to the particle mode heat transfer with the extended surface were higher than the coefficients calculated from the bare tube surface.

3. With local heat transfer coefficients and experimentally determined sectional particle fractions over the 11 different sections of the fluidized bed, Nusselt numbers were correlated with an equation based on a particle mode heat transfer mechanism.

4. It is concluded that particle Nusselt numbers are proportional to 0.48 of I-ε.

Statement of Permission to Copy

In presenting this thesis in partial fulfillment of the requirements for an advanced degree at Montana State University, I agree that the Library shall make it freely available for inspection. I further agree that permission for extensive copying of this thesis for scholarly purposes may be granted by my major professor, or, in his absence, by the Director of Libraries. It is understood thay any copying or publication of this thesis for financial gain shall not be allowed without my written permission.

Signature Joon Taik Kim

Date Feb. 27, 1970

HEAT TRANSFER IN THE FINNED FLUIDIZED BED TUBULAR HEAT EXCHANGER

By

JOON T. KIM

A thesis submitted to the Graduate Faculty in partial fulfillment of the requirements for the degree

of

MASTER OF SCIENCE

in

Chemical Engineering

Approved:

Lloyd Berg
Head, Major Department

William E. Veneth
Chairman, Examining Committee

K. Loening
Graduate Dean

MONTANA STATE UNIVERSITY
Bozeman, Montana

March, 1970

N378
K562
Cop. 2

VITA

Joon Taik Kim, the author, was born March 17, 1945, in Seoul, Korea. He is the son of Mr. Chang Hwa Kim and Mrs. Young Ja Chun. He received his elementary and secondary education at Seoul, Korea. He graduated from Pai Chai High School in February, 1963. In March, 1963, he enrolled at Yonsei University in Seoul, Korea, and graduated February, 1967 with a B. S. degree in Chemical Engineering. From January, 1967 to September, 1968, he worked with the Medium Industry Bank as a technical services engineer and conducted various feasibility studies on AID and OECF loan granted industries specializing in gas conversion.

He enrolled in Chemical Engineering Department at Montana State University as a research assistant in September 1968 working toward Master of Science degree.

ACKNOWLEDGEMENTS

I would like to thank Dr. William E. Genetti of Montana State University for his assistance and encouragement throughout the duration of the investigation. I wish to express my gratitude to Mr. Ronald D. Aafedt for his assistance which helped me to complete my study. I would like to thank Miss So Young Hahn for her heartful help to finish my study and research. Special thanks go to my parents for their encouragement throughout the period of research.

I wish to acknowledge the financial support I received from the Engineering Experiment Station at Montana State University.

TABLE OF CONTENTS

		Page
I.	Introduction	1
II.	Literature Survey and Theory	3
III.	Experimental Apparatus	28
IV.	Experimental Procedure	45
V.	Calculations	48
VI.	Analysis of Data	53
VII.	Results and Conclusion	80
VIII.	Literature Cited	83

APPENDICES

Appendix I	Nomenclature	86
Appendix II	Evaluation of η and R	93
Appendix III	A Typical Data Sheet	95
Appendix IV	Calibration Tables for Thermocouples	97
Appendix V	Complete Data (Table IV)	119

LIST OF FIGURES

		Page
Figure 1.	Solid movement and gas flow as visualized by bubbling bed model.	7
Figure 2.	Correlation for heat transfer between containing wall and fluidized bed	18
Figure 3.	Correlation for heat transfer between internal vertical tubes and fluidized bed.	19
Figure 4.	Correction factor C_R for non axial location of immersed tubes.	20
Figure 5.	ICPP multiple-tube data compared with Vreedenberg's correlation for heat transfer to a single tube	22
Figure 6.	Flow diagram of the fluidizing apparatus	29
Figure 7.	(A) General Equipment (B) Glass particles	31
Figure 8.	Tube layout: showing locations of heating element.	34
Figure 9.	Diagram of electrical circuit.	36
Figure 10.	Exploded view of the tube wall temperature probe.	39
Figure 11.	Average Nusselt numbers correlation without fluidization.	54
Figure 12.	Vertical fluidized bed temperature profiles	56
Figure 13.	Local heat transfer coefficients.	59
Figure 14.	Local heat transfer coefficients	61
Figure 15.	Local heat transfer coefficients	63

Figure 16.	Local heat transfer coefficients.	64
Figure 17.	Local heat transfer coefficients.	66
Figure 18.	Local heat transfer coefficients.	68
Figure 19.	Local heat transfer coefficients.	70
Figure 20.	Local heat transfer coefficients.	71
Figure 21.	Average sectional coefficients for batch fluidization	73
Figure 22.	Correlation for average contact time.	77
Figure 23.	The present modified correlation for sectional particle Nusselt numbers.	79
Figure 24.	The correlation for η and R.	93
Figure 25.	Nomograph to calculate G_{mf}	94

LIST OF TABLES

		Page
Table I.	Experimental Program	44
Table II.	Difference of Local Heat Transfer Coefficient Between Different Extended Surfaces	65
Table III.	The Weighted Average Contact Times	74
Table IX	Complete Data	119-142

ABSTRACT

Local and average heat transfer coefficients for bed-to-wall heat transfer from a fluidized bed tubular heat exchanger with extended surfaces were investigated.

The fluidized bed tubular heat exchanger consisted of a 44-inch long, 5.5-inch inside diameter shell with 19, 3/4-inch diameter stainless steel tubes arranged in a 1-inch triangular pitch. Air was used as the fluidizing medium and glass spheres of 0.0185-inch average diameter were used in this study.

Tubes at the four possible tube locations tube were heated electrically. 3/16-inch stainless steel wire was used as an extended surface. The stainless steel wire was wrapped around the outside of each 19 tubes in a helical sprial. Variables studied include particle concentration, gas mass velocity and twist ratio.

The Results of This Study Are as Follows

1. Gradual increase in the weighted average heat transfer coefficients with respect to the number extended surface were observed. Local heat transfer coefficients decreased with the distance from the entrance of the fluidized bed. Tube locations had only a slight effect on local heat transfer coefficients.
2. The average sectional coefficients according to the particle mode heat transfer with the extended surface were higher than the coefficients calculated from the bare tube surface.
3. With local heat transfer coefficients and experimentally determined sectional particle fractions over the 11 different sections of the fluidized bed, Nusselt numbers were correlated with an equation based on a particle mode heat transfer mechanism.
4. It is concluded that particle Nusselt numbers are proportional to 0.48 of $1-\varepsilon$.

Introduction

The study of design methods for improved fluidized bed heat exchangers as industrial heat transfer equipment has become greatly important, because of its isothermal characteristic along with various applications in chemical and physical operations.

Fluidization is the phenomenon in which the gravitational force acting on a dense packet of particles is counteracted by an upward fluid stream, which causes these particles to be kept more or less in a floating state. The uniform temperature distribution of the fluidized bed is due to the turbulent fluid-solids suspended motion and the continuous, frequent contacts between the heating surface and a new swarm of particles by the rapid circulation of the fluidized stream.

Even if the fundamentals of fluidization were not fully and completely understood, many fluidized-solids processes have achieved commercial success. Fluid-bed catalytic cracking units with the conversion level of 50-60 percent is an example. The need for heat, mass, and momentum transfer correlations in fluidized beds was paramount for fluidized bed techniques to be a success.

One of the noticeable advantages of fluidized-beds to one-phase flow is high rates of heat transfer. It is well-

known that higher heat transfer coefficients can be achieved with extended surfaces, however, this effect is sometimes dismissed as a means to improve performance of aheat exchanger because of the correspondingly higher power consumption.

Numerous studies have been made to find out the effect of various types of extended surfaces on the rate of heat transfer in turbulent flow for different industrial heat transfer equipment. These results are in no way general, but it is at least evident that extended surfaces like spiral wires or twisted strips have some effects on increasing the rate of heat transfer in industrial heat transfer equipment for single phase systems.

A number of studies on local and average heat transfer coefficients for heat transfer from an internal tube in a bundle of tubes to a fluidized-bed have been made. The present investigation is a study of local and average heat transfer rates in the fluidized bed tubular heat exchanger with the extended surfaces. Local heat transfer coefficents were measured with a moving thermocouple probe inside an electrically heated tube. This probe made it possible to measure local heat transfer coefficients at any point along a tube for various gas rates and particle concentrations. The rate of heat transfer was correlated with the area of extended surfaces.

Literature Survey and Theory

Fluid Mechanical Approach of Fluidized Beds

By assuming a fully developed circular bubble and solid-free, spherical in the three-dimensional case, cylindrical in the two-dimensional case, Davidson (3) adopted a continum approach, potential flow for both the fluid and particulate phases to postulate the motion of rising bubble. Even if Davidson model was not sufficiently accurate, it was the first useful approach to the motion of a rising bubble in the gas-solid fluidized bed.

Murray (17) adopted a continum approach for the two-phase motion of the fluid and solids in a fluidized bed. Momentum and mass conservation equations were applied to obtain solutions for the motion caused by rising bubbles in the bed. The stability analysis and the equations had been derived to provide a means of classifying fluidized systems, but he did not evaluate the roots of his secular equation, so that no quantitative results were obtained.

Anderson and Jackson (1) realized that for practical purposes it is necessary to seek some method of simplifying the actual problem so that it can be described by a small system of partial differential equations. Anderson and Jackson have used a formal mathematical definition of local mean variables to translate the point Navier-Stokes equations

for the fluid and the Newtonian equations of motion for the particles somewhat devoid of number of terms whose forms are yet undetermined.

According to the renewal model proposed by Mickley and Fairbanks (18), owing to the bubbles, packets of particles are renewed continuously between the bulk of the bed and the vicinity of the wall. The rate of heat transfer between a non-homogeneous fluidized bed and a wall depends on the thermal conductivity of these packets and on their renewal frequency.

It appears a quantity, the renewal frequency ω, to be determined more specifically according to a more complete representation of hydrodynamic process. If the swarm of solid particles is assimilated to a quasi-fluid it is possible to write the equation of motion for the two-phase system. A volume which is encountered here is sufficiently small to be considered as infinitely small, but also large enough to contain a sufficiently large number of particles. Ruckenstein (24) suggested that a synthesis between the renewal model and the linearized instability theory might be able to give information with respect to the renewal frequency. The experimental results of Mickley and Fairbanks (18) show that ω is in the range 1 - 10 sec^{-1} and that it does not depend too much on the fluidization velocity. For

glass spheres of 10^{-4} meter diameter Ruckenstein (24) computed that the renewal frequency is about 4 sec^{-1} and predicted a weak dependence of ω on velocity.

Newly Proposed Bubble-bed Model in Heat Transfer

Several theoretical mechanisms of fluidized bed models have been proposed and some of those have been briefly summarized by Genetti (8) for heat transfer in order to provide a basis for understanding correlations which have been presented in his recent work.

Kunii and Levenspiel (11, 12) have proposed a model for the flow of gas through a fluidized bed, the bubble-bed model, or a three-region model which have viewed as uniformly sized bubbles surrounded by clouds and followed by wakes. A sketch of this model is given in Fig. 1. They have shown that this model is good enough to fit the reported data for gas-solid heat transfer, gas-solid mass transfer and conversion in catalytic reactions.

Kunii and Levenspiel have only been concerned with the dense bubbling region. This region applies where a continuous exchange or floowing up of solid particles along the heat transfer surface is continuing. This concept has been sometimes explained on the basis of the "packet"theory (9).

For the bubble phase, Kunii and Levenspiel have started with several necessary assumptions to simplify the problem from the Davidson model (4). They have taken the bubble size to be uniform throughout the bed or section of bed and called it the effective bubble size. The velocity of rise of a crowd of bubbles has been related to the velocity of rise of

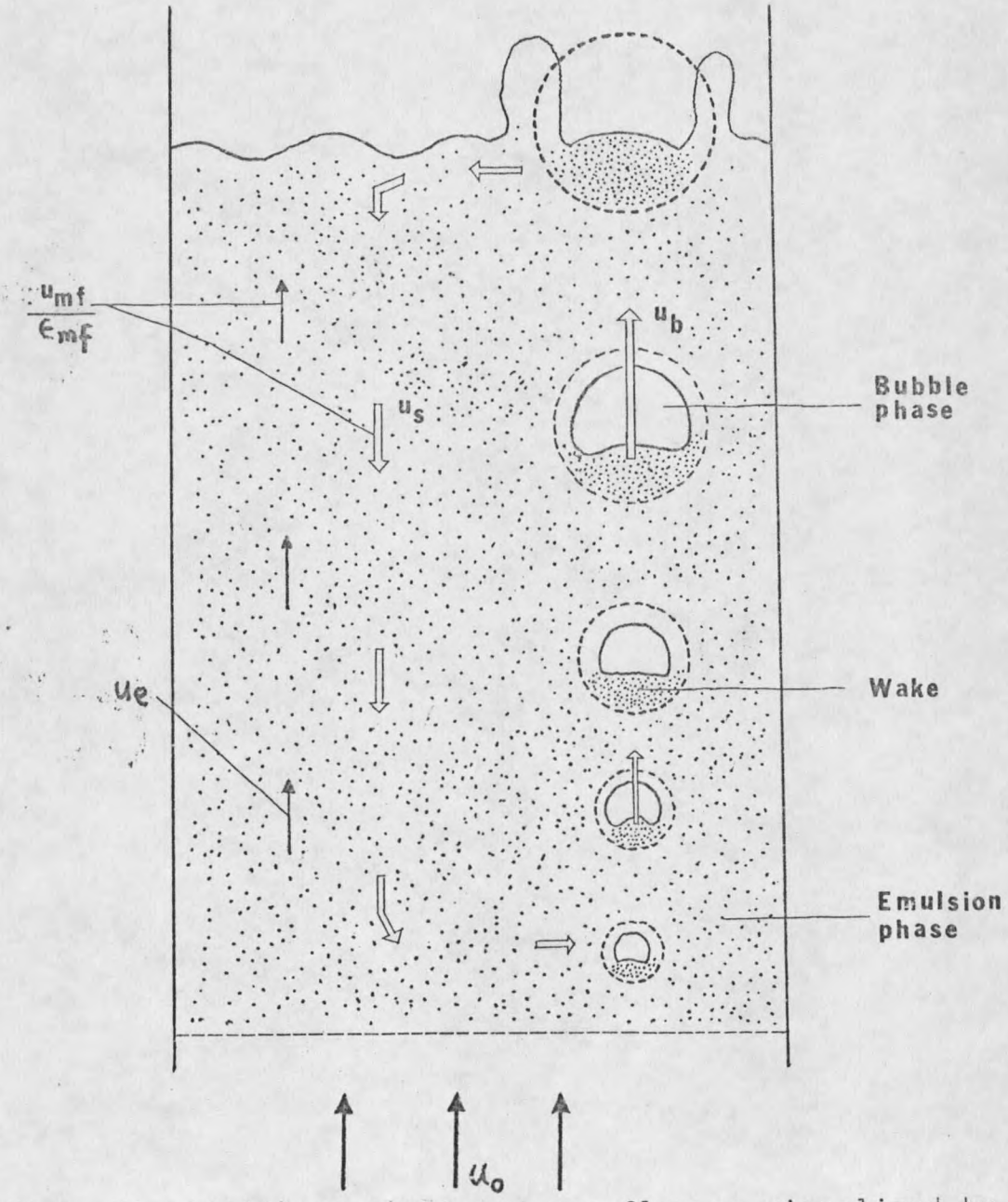


Figure 1. Solid movement and gas flow as visualized by bubbling bed model.

a single bubble by

$$u_b = u_o - u_{mf} + u_{br} = u_o - u_{mf} + 0.711(gd_b)^{\frac{1}{2}} \qquad (1)$$

where $u_{br} = 0.711(d_b)^{\frac{1}{2}}$.

Ignoring small amounts of solids inside the rising bubble (measured to be from 0.2% to 1% by different investigators), they have taken the bubble void fraction $\varepsilon_b = 1$. The average bed voidage ε_f has been related to the voidage in bubbles and emulsion phase by

$$\varepsilon_f = \delta\varepsilon_b + (1-\delta)\varepsilon_e = \delta + (1-\delta)\varepsilon_e \qquad (2)$$

where δ = the volume fraction of bubbles in the bed.

By assuming $\varepsilon_e = \varepsilon_{mf}$, voidages and bed heights have been correlated by

$$1 - \delta = \frac{L_{mf}}{L_f} = \frac{1 - \varepsilon_f}{1-\varepsilon_{mf}} \text{ and } \frac{L_{mf}}{L_m} = \frac{1 - \varepsilon_m}{1 - \varepsilon_{mf}} \qquad (3)$$

The bubble phase variables d_b, u_b and δ have been correlated to give u_o and u_{mf}, i.e.

$$u_b = \frac{u_o - (1-\delta)u_{mf}}{\delta} \cong \frac{u_o - u_{mf}}{\delta}$$

For the emulsion phase, Kunii and Levenspiel (11,12) have assumed the void fraction of the wake to be that of the emulsion phase and have correlated the relative velocity of upward percolating gas, u_e, and of downward flowing solid,

u_s, to the superficial gas velocity of minimum fluidization, u_{mf};

$$u_e = u_f - u_s = \frac{u_{mf}}{\varepsilon_{mf}} - u_s. \qquad (5a)$$

The downward velocity of solid is given by

$$u_s = \frac{\alpha\delta\, u_b}{1-\delta-\alpha\delta}$$

$$\text{where } \alpha = \frac{\text{volume of wake dragged up to the bed behind a rising bubble}}{(\text{volume of bubble})}.$$

Variables d_b, u_b, δ, u_e, and u_s have been correlated to give u_o and u_{mf}, i.e.

$$u_b = \frac{1}{\delta}\,[u_o - (1 - \delta - \alpha\delta)u_{mf}]. \qquad (6)$$

Equation 6 has been approximated to give the expression for the whole range of flows, and the result is identical to Equation 4;

$$u_b \cong \frac{u_o - (1-\delta)u_{mf}}{\delta} = \frac{u_o - u_{mf}}{\delta}. \qquad (7)$$

Bed-to-Wall Heat Transfer in Gas-Solid Fluidized Beds

Much work has been done on bed-to-wall heat transfer for numerous heating surface arrangements. Empirical equations have been developed to predict heat transfer coefficients for heat transfer from these surfaces.

Frantz (7) has summarized work done on surface-to-bed heat transfer in fluidized beds. Genetti (8) has discussed numerous proposed correlations and several heat transfer mechanisms for fluidized bed heat transfer.

Usually fluidized systems have low enough absolute temperatures so that thermal radiation may be safely discounted as a significant contributing factor. However, in many metallurgical applications of the fluidized bed techniques the processing temperatures are sufficiently high so that thermal radiation may be an important part of the over-all heat transfer process. Szekeley and Fisher (25) recently have studied bed-to-wall radiation heat transfer on the basis of the study of bed-to-wall heat transfer in the convective regime done by Botterill and et al (2).

While none of the proposed mechanisms has been sufficient to predict heat transfer coefficients for many different situations encountered, various mechanisms explaining the high rates of heat transfer between

exchanger walls and fluidized beds have been suggested, and can be classified as follows:

(1) van Heerden et al (10) and Wicke and Fetting (32): the fluidizing medium (gas) acted as a stirring agent and the solids transported most of the heat, and the fluidized bed was visualized as well stirred liquid. Therefore, there is the steady state conduction through the emulsion phase.

(2) Leva et al (15), Dow and Jakob (5) and Levenspiel and Walton (16): the scouring action of the solids along the heat exchanger wall reduces the thickness of the laminar gas film and increases the rate of heat transfer.

(3) Mickley and Fairbanks (18): the fluidized bed was assumed to be composed of "packets" which renewed intermittently by the violent disturbance in the core portion of the fluidized bed, and where unsteady-state diffusion of heat to newly arrived mobile elements occurred.

(4) Ziegler et al (34) and Botterill and Williams (2): unsteady-state conduction by single particles in direct contact with heat exchanger walls. This model has been further modified by Genetti (8) to give more complete predictions with respect to experimental data.

This modified model is adopted in the present work. The results of this model predict two established facts. The Nusselt number is independent of thermal conductivity of the solids (19,34) and is proportional to about the square root of the particle fraction, $1 - \varepsilon$ (20). The results of the model also predict a maximum Nusselt number, which also is an established fact (15).

1. A Rather Different Explanation According to the Bubble Bed Model

Yoshida, Kunii, and Levenspiel (33) have tried to unify the mechanisms proposed by Mickley and Fairbanks (18), and van heerden et al (10) and Wicke and Fetting (32), and have applied the bubble model to postulate bed-to-wall heat transfer. However, the work is not complete, and some of the quantitative parameters are still not well-known.

They have started the prediction of the basis of the film-penetration theory for gas absorption into liquids proposed by Toor and Marchello (26). The equation which represents this film-penetration model for mass and heat transfer[1] is

$$\frac{\partial T}{\partial T} = \alpha \frac{\partial^2 T}{\partial^2 T} \qquad 0 \leq x \leq l_e$$

where $$\alpha = \frac{k_e}{\rho_e C_{ps}} = \frac{k_e}{\rho_s C_{ps}(1-\varepsilon_{mf})}$$

l_e = effective thickness of emulsion layer.

---

[1] A thin layer of emulsion of thickness l_e suddenly contacts the exchanger wall and after a short time it is suddenly moved away to replace a fresh element of emulsion from the core portion of the bed. Therefore it will include the steady state conduction of heat through an emulsion layer at the wall and the unsteady state absorption of heat by emulsion elements.

And boundary conditions are

$$T = T_b \text{ at } t = 0$$

$$T = T_w \text{ at } x = 0$$

$$T = T_b \text{ at } x = l_e$$

The solution of the above equation is

$$\frac{T_w - T}{T_w - T_b} = 2 \sum_{n=1}^{\infty} (-1)^{n+1} \frac{\sin n\pi(1 - x/l_e)}{n\pi} \exp\left(-n^2\pi^2 \frac{a\,t}{l_e^2}\right) \qquad (9)$$

From the above solution, the instantaneous local heat transfer coefficient is found to be

$$h_{ti} = \left[\frac{k_e \rho_e C_{ps}}{\pi t}\right]^{1/2} \left[1 + 2 \sum_{n=1}^{\infty} \exp\left(-\frac{n^2 l_e^2}{at}\right)\right]$$

$$= \frac{k_e}{l_e} \left[1 + 2 \sum_{n=1}^{\infty} \exp\left[n^2\pi^2 \frac{a\,t}{l_e}\right]\right] \qquad (10)$$

The observed coefficient of heat transfer h_w is the time averaged value of the instantaneous coefficient, and that is given by

$$h_t = \int_0^{\infty} h_{ti}\, I(t)\, dt \qquad (11)$$

where $I(t)$ = the age distribution function of emulsion elements on the surface.

Two types of age distribution functions have been considered: Case 1. random surface renewal, and Case 2. uniform surface renewal. A number of expressions for the observed heat transfer coefficients, h_w, have been derived according to the different criterions.

The bubbling bed model gives a simple representation of bubble flow, the emulsion flow and the interaction of these streams. However, two empirical expressions which have been reported by Wen and Leva (31) and Wender and Cooper (30). are usually recommended for the design of the bed-to-wall heat transfer.

2. Some Generalized Design Equations for Wall-to-Bed Heat Transfer

Bed-to-exterior wall heat transfer:

Wen and Leva (31) attempted to correlate some earlier observations of solids motion in the bed with heat transfer phenomena through a boundary layer. They considered that the chief resistance to heat exchange between a containing wall and a fluidized bed is in the laminar film at the vessel boundary. The thickness of the film is influenced by the velocity of particles along the wall parimarily due to the "scouring action" of the particles. By the usual method of plotting and cross plotting, the following relation was

obtained:

$$\frac{hd_p}{k} = 0.16 \left(\frac{C_s \rho_s d_p^{1.5} g^{0.5}}{k}\right)^{0.4} \left(\frac{G_f k_p \eta}{\mu R}\right)^{0.36} \quad (12)$$

where η = the fluidization efficieny

R = the bed expansion ratio.

Nomographic solutions for evaluation of η and R have been given in Appendix II. Wender and Cooper (30) made a curve of the dimensionless group Y/F with the paricle Reynolds number as shown in Figure 2 with five data sets included. The term Y and F are defined as:

$$Y = \left(\frac{h D_p}{k[1-\varepsilon]}\right) \left(\frac{C_g \rho_g}{C_s \rho_s}\right) \quad (13)$$

$$F = 1 + 7.5e^{-0.44} \left(\frac{L_h}{D_t}\right) \left(\frac{C_g}{C_s}\right) \quad (14)$$

Bed-to-interior wall heat transfer:

Internal, vertical-tube heat transfer was found to be independent of tube length, particle shape and particle size distribution. Wender and Cooper (30) made a straight line plot of the dimensional Z/C_R group with the particle Reynolds number as shown in Figure 3 with six data sets included for the internal vertical heat transfer surface. The term Z is defined as:

$$Z = \frac{(hd_p/k_g)(k_g/C_g\rho_g)^{0.43}}{(1-\varepsilon)(C_s/C_g)^{0.80}\,(\rho_s/\rho_g)^{0.66}} \qquad (15)$$

The term C_R allows for non-axial tube location and may be evaluated from Figure 4 which originally was given by Vreedenberg (28). The equation of this correlation is:

$$\left(\frac{hd_p}{k[1-\varepsilon]}\right)\left(\frac{k}{C_g\rho_g}\right)^{0.43} = 0.33C_R\left(\frac{d_pG}{\mu}\right)^{0.23}\left(\frac{C_s}{C_g}\right)^{0.80}\left(\frac{\rho_s}{\rho_g}\right) \qquad (16)$$

Noë and Knudsen (22) have made a study of heat transfer from a vertical tube located in a bundle of vertical tubes in a fluidized bed. Their data was compared to the correlation of Wender and Cooper (30) using a value of $C_R = 2$. Almost all their experimental data was within $\pm$ 50 percent of the correlation. This is fair agreement considering the greatly different geometries.

Immersed, horizontal-tube heat transfer has been studied by Vreedenberg (29) along with the effect of tube diameter, particle size, shape, and density, and gas velocity on the heat transfer coefficient, including data on large-scale beds. The recommended correlations are:

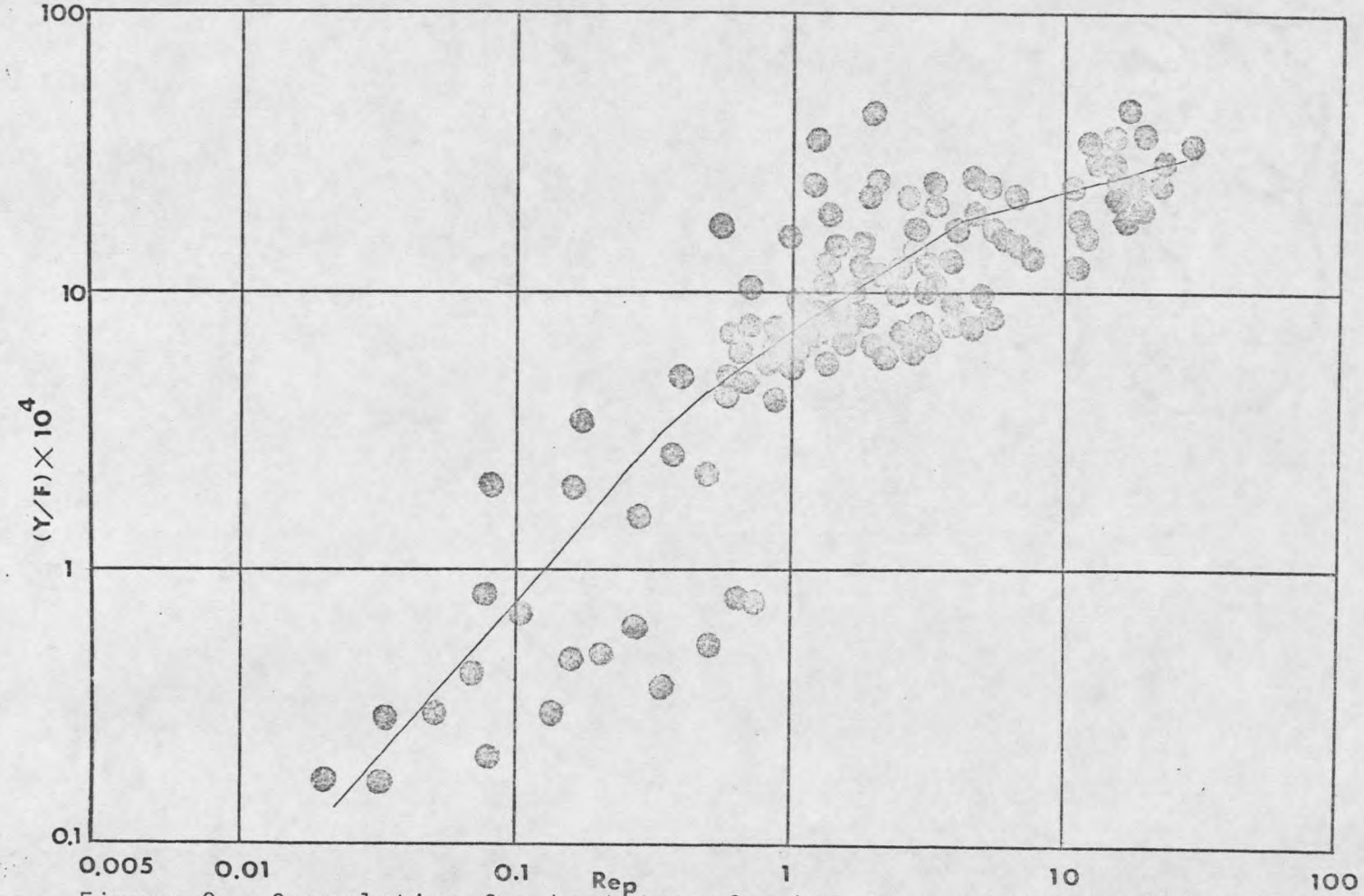


Figure 2. Correlation for heat transfer between containing wall and fluidized bed.

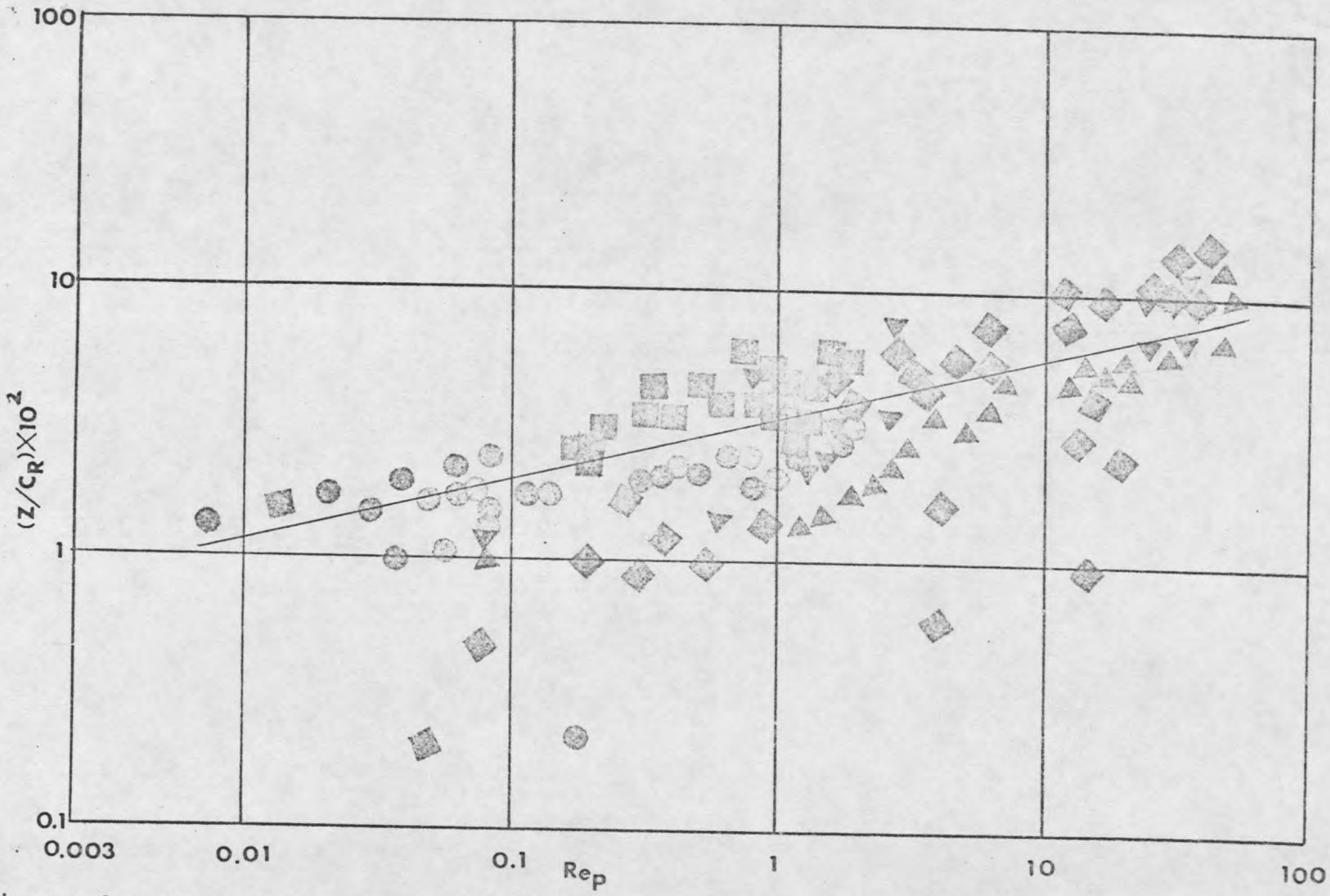


Figure 3. Correlation for heat transfer between internal tubes and bed.

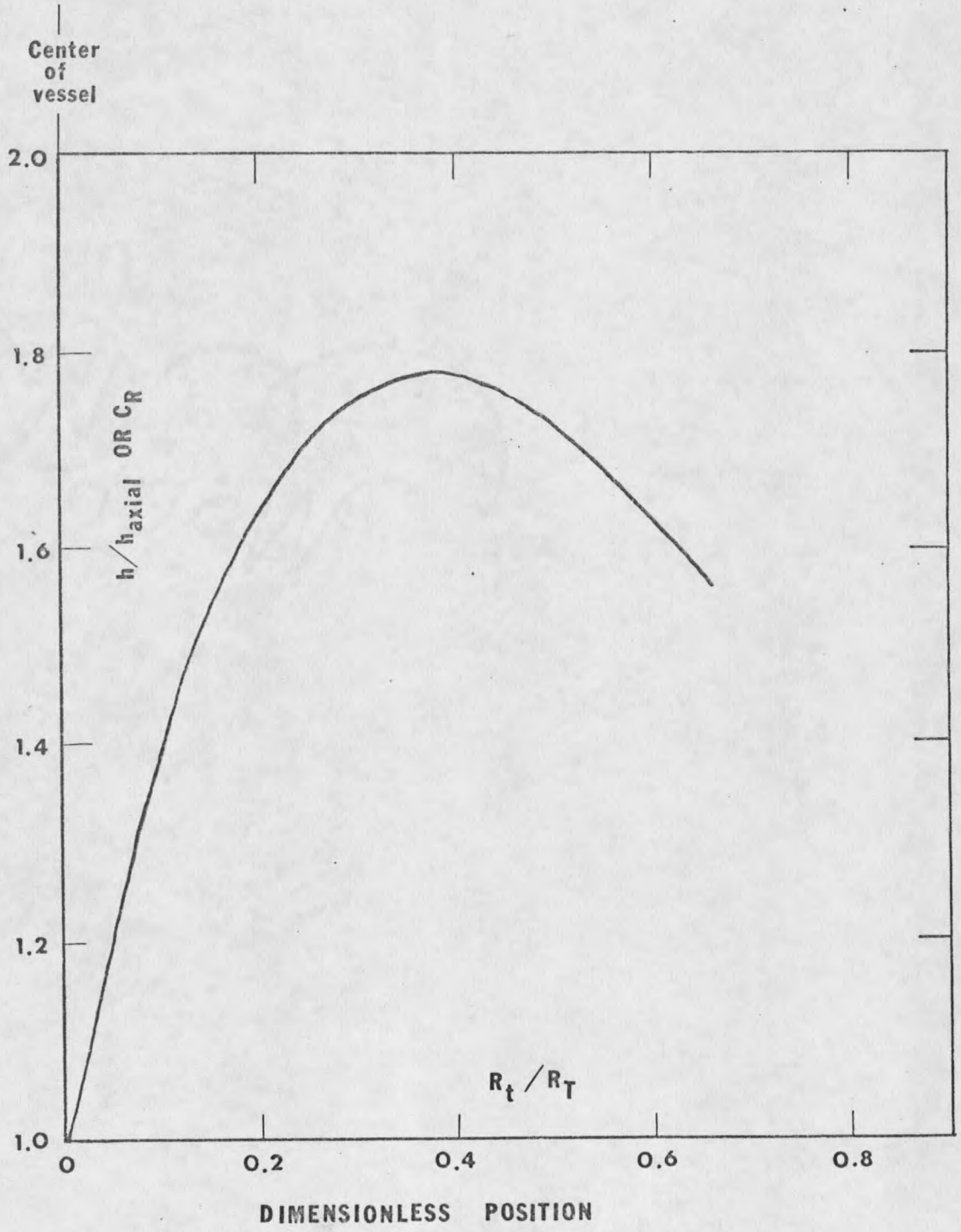


Figure 4

Correction factor C_R for nonaxial location of immersed tubes.

$$\frac{h_w d_{ti}}{k_g} = 0.66 \left(\frac{C_{pg}}{k_g}\right)^{0.3} \left[\left(\frac{d_{ti}\rho_g u_o}{\mu}\right)\left(\frac{\rho_s}{\rho_g}\right)\left(\frac{1-\varepsilon_f}{\varepsilon_f}\right)\right]^{0.44} \quad (17)$$

for Reynolds number less than 2,000,

and

$$\frac{h_w d_{ti}}{k_g} = 420 \left(\frac{C_{pg}\mu}{k_g}\right)^{0.3} \left[\left(\frac{d_{ti}\rho_g u_o}{\mu}\right)\left(\frac{\rho_s}{\rho g}\right)\left(\frac{\mu^2}{d_p{}^3 \rho_s g}\right)\right]^{0.3} \quad (18)$$

for Reynolds number greater than 2,500.

Petrie, Freeby, and Buckham (28) have proposed the correlation best fitting ICPP[1] data for heat transfer from the various non-finned multiple horizontal tube bundles in the fluidized bed heat exchanger. That is

$$Nu_t = 14\left(\frac{G}{G_{mf}}\right)^{1/3} (Pr)^{1/3} \left(\frac{D_t}{d_p}\right)^{2/3} \quad (19)$$

The experimental data shows a maximum deviation of 64 percent from Vreedenberg's correlation, while Equation 19 fits the data better. However, the agreement of the proposed data with Vreedenberg's correlation for heat transfer to a single tube is good. Their data is shown in Figure 5.

---

[1]The Atomic Energy Commission's Idaho Chemical Processing plant.

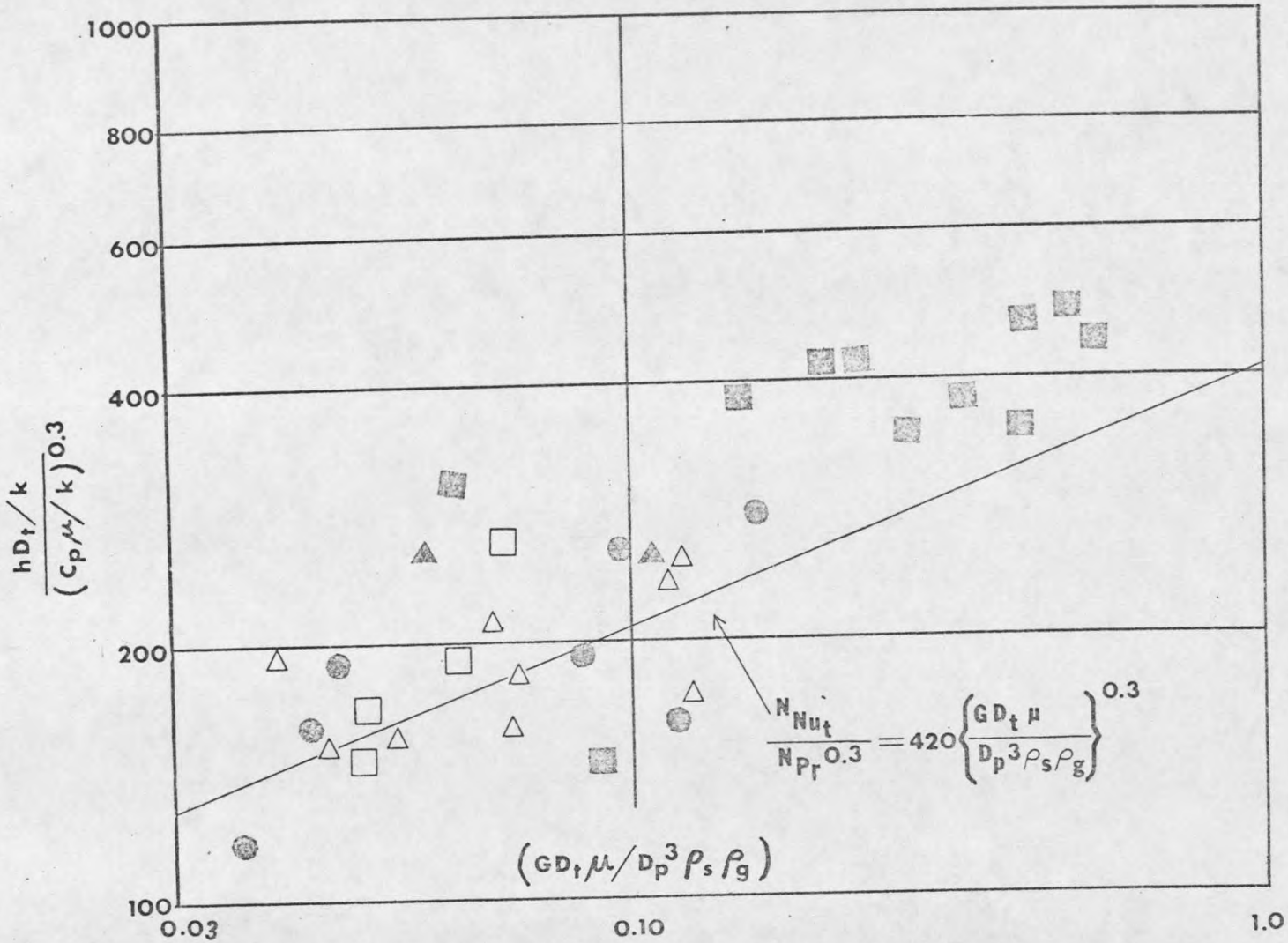


Figure 5. 1CPP multiple-tube data compared with Vreedenberg's correlation.

3. Correlation Model, Used in This Work, For Wall-to-Bed Heat Transfer

The model initially suggested by Ziegler et al (34) and Botterill and Williams (2) further extended by Genetti (8) is modified in this present study. Ziegler, Koppel, and Brazelton (34) showed that the wall-to-bed heat transfer coefficients varied with solid heat capacity, C_{ps}, but was independent of solid thermal conductivity, k_s.

A particle which has been in the bulk medium is viewed to move adjacent to the wall surface where the particle is suddenly bathed by the fluid adjacent to the wall at the wall temperature. In the mean time the particle receives heat by convection from the fluid adjacent to the wall. After sometime the particle leaves the wall and returns to the bulk fluidized medium. The major portion of heat transfer is assumed to occur by this mechanism. With several assumptions the boundary problem describing the temperature profile, $T(r,\theta)$, in a particle while it is adjacent to the wall is solved. The time averaged heat flux is obtained as:

$$\bar{q}_p = \frac{\pi d_p k_g (T_w - T_b)}{(1 + \frac{M\bar{\theta}}{2})^2} \qquad (20)$$

where $\bar{\theta}$= the average contact time

$$M = \frac{12k_g}{\rho_s C_s d_p^2}$$

In order to get the expression for the heat transfer flux based on the wall surface, the number of particles at the surface per unit area will have to be derived. The number of particles per unit area, γ_p, will be related to the particle fraction, $1-\varepsilon$, and the particle diameter. The heat transfer coefficient has been calculated to be proportional to $(1-\varepsilon)^{0.48}$. A relation of the following form is proposed:

$$\gamma_p = K_1(1-\varepsilon)^{0.48} f(d_p). \tag{21}$$

For a completely covered surface with hexagonal packing, γ_p, and $1-\varepsilon$ are

$$\gamma_p = \frac{2/3}{d_p^2} \tag{22}$$

$$1 - \varepsilon = 14/27 \tag{23}$$

Therefore

$$K_1 = 1.59 \tag{24}$$

and

$$f(d_p) = \frac{1}{d_p^2} \tag{25}$$

By substituting Equation 24 and Equation 25 into Equation 21, we can get the following expression for γ_p:

$$\gamma_p = \frac{1.59(1-\varepsilon)^{0.48}}{d_p^2} \tag{26}$$

By multiplying q_p by γ_p, we can write an equation for the heat flux from the wall surface:

$$q = \gamma_p q_p = \frac{5.0(1-\varepsilon)^{0.48} k_g (T_w - T_b)}{d_p \left(1 + \frac{6k_g \bar{\theta}}{\rho_s C_s d_p^2}\right)^2} \tag{27}$$

The particle Nusselt number is

$$Nu_p = \frac{5(1-\varepsilon)^{0.48}}{\left(1+\frac{6k_g \bar{\theta}}{\rho_s C_s d_p^2}\right)^2} \tag{28}$$

With the aid of dimensional analysis Genetti (8) has introduced the following equation for $\bar{\theta}$

$$\bar{\theta}\left(\frac{g}{D_p}\right)^{1/2}\left(\frac{\rho_g}{\rho_s}\right)^{1.1} Re_p = 97 \left(\frac{G_{mf}}{G}\right)^{4/3} \tag{29}$$

By substituting $\bar{\theta}$, as expressed in Equation 29, into Equation 28, the following correlation for average Nusselt numbers can be obtained:

$$Nu_p = \frac{5\,\phi(1-\bar{\varepsilon})^{0.48}}{\left[1 + \frac{580}{Re_p}\left(\frac{k_g}{D_p^{3/2} C_s \rho_s g^{1/2}}\right)\left(\frac{\rho_s}{\rho_g}\right)^{1.1}\left(\frac{G_{mf}}{G}\right)^{4/3}\right]^2} \qquad (30)$$

Most of the data calculated by Genetti for fluidization with the coarse glass spheres and the aluminum particles are within ±20 percent of Equation 30.

Kidd (14) has studied heat transfer and pressure drop for nitrogen flowing in tubes containing twisted tapes and has introduced twist ratio Y. Twist ratio Y has been defined as the number of tube diameter per 180° twist.

About the constant of Equation 28 as a result of several assumptions Genetti (8) has reported 5. For generalization Equation 28 can be rewritten:

$$Nu_p = \frac{C_1(1-\varepsilon)^{0.48}}{\left(1 + \frac{6k_g\bar{\theta}}{\rho_s C_s d_p^2}\right)^2} \qquad (31)$$

The dimensionless group $\frac{6k_g\bar{\theta}}{\rho_s C_s d_p^2}$ in Equation 31 can be related to the following variables:

1. mass velocity G
2. particle diameter d_p
3. twist ratio Y
4. gas viscosity μ

With the aid of dimensional analysis the following dimensionless group can be obtained:

$$\left(\frac{D_p G}{\mu}\right), \quad \left(\frac{Y-1}{Y}\right)$$

With these groups an equation of the following form for the dimensionless group $\frac{6k_g\bar{\theta}}{\rho_s C_s d_p^2}$ is obtained:

$$\frac{6k_g\bar{\theta}}{\rho_s C_s d_p^2} = \frac{1}{2}M = C_2\left(\frac{D_p G}{\mu}\right)^{-a}\left(\frac{Y-1}{Y}\right)^{b} \qquad (32)$$

Substituting Equation 32 into Equation 31, the following is obtained:

$$Nu_p = \frac{C_1(1-\varepsilon)^{0.48}}{\left[1 + \frac{C_2\left(\frac{Y-1}{Y}\right)^{b}}{Re_p^{a}}\right]^2} \qquad (33)$$

Experimental Apparatus

The experimental equipment of the present investigation was designed and assembled in order that the study of local and average heat transfer coefficients could be made in a fluidized bed tubular heat exchanger where an electrically heated bundle of verticle tubes were symmetrically placed. Some of the equipment components used in this present study were used in a previous study undertaken by Genetti (8). The major items of equipment are a model fluidized bed heat exchanger, an air blower, an electrical system and power source, and measuring devices. The measuring devices include manometers, thermocouples and a precision potentiometer. A general flow diagram of the equipment is shown in Figure 6 and a photograph of the equipment is shown in Figure 7 (A).

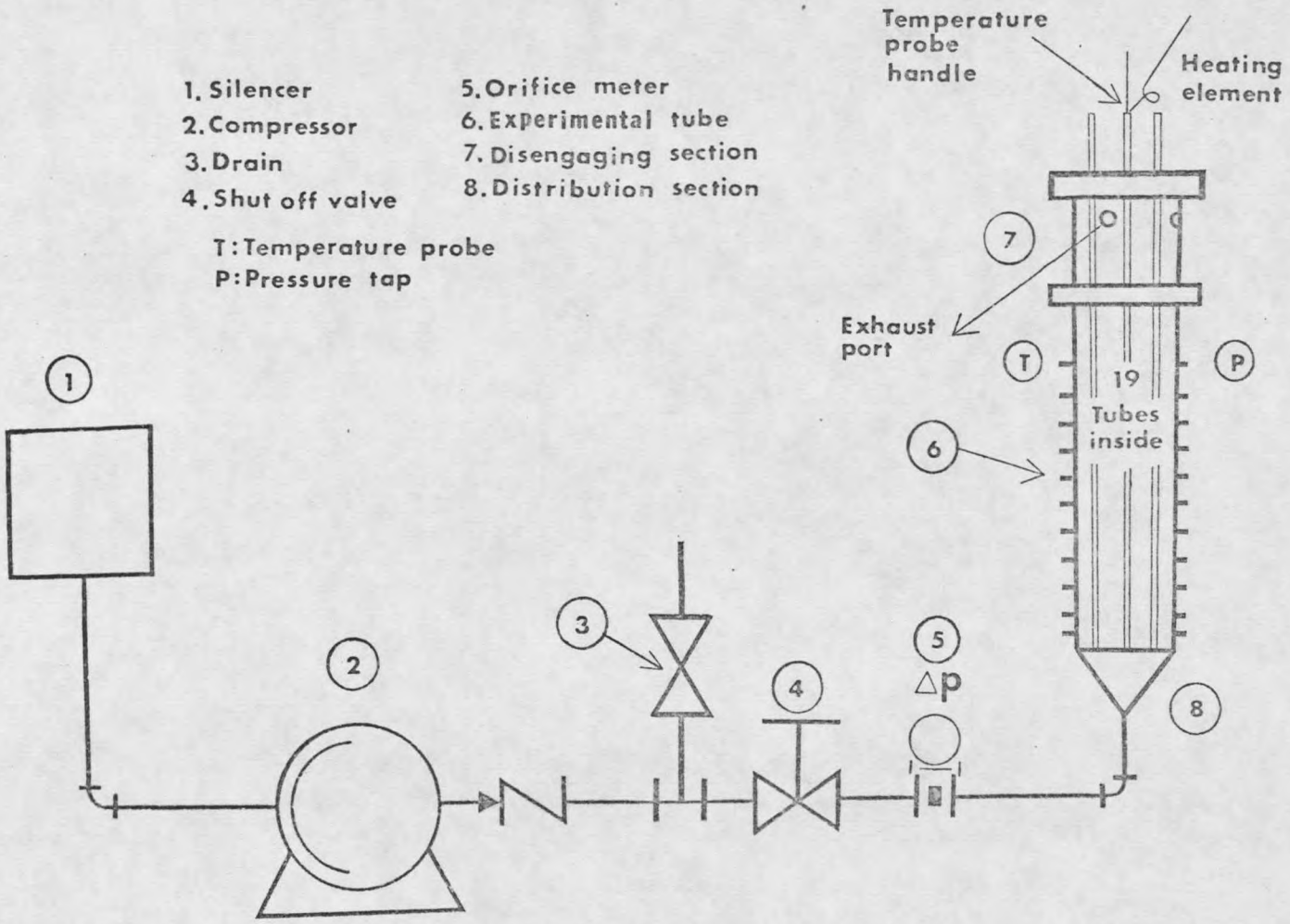


Figure 6. Flow diagram of the fluidizing apparatus.

The Experimental Heat Exchanger Column

The experimental heat exchanger column consisted of a vertical tube bundle containing heating elements and a shell.

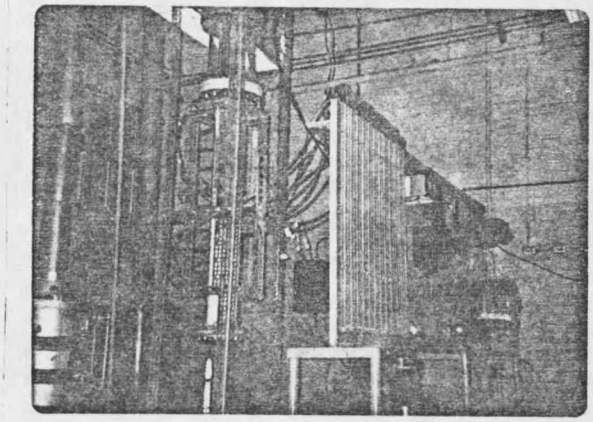
The Experimental Shell: The outside of the experimental shell was constructed in three sections, the conical air distributing section, the experimental section, the disengaging section.

The conical air distributing section is attached at the lower part of the column to expand the air flow from the pipe diameter to the column diameter. A iron-constantan thermocouple was inserted through the wall of this section to measure the air inlet temperature.

The experimental section was constructed from the 6-inch OD and 44-inch long cast acrylic tube with the 1/4 inch thick wall. Eleven iron-constantan thermocouples were inserted through the wall of this experimental column as shown in Figure 6. The thermocouples are protected by screen shields in order to give contact with the fluidizing air only. Eleven pressure taps are also placed in the wall of this experimental column as shown in Figure 6. These pressure taps have fine screen covers soldered on to prevent the fluidized particles from running into the taps.

The disengaging section was constructed from the 9-inch

(A)



(B)

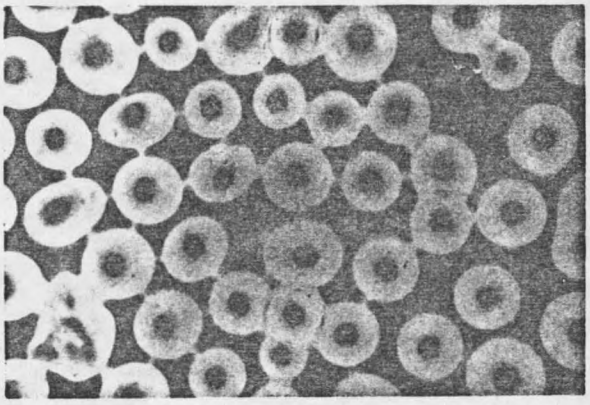


Figure 7. (A) General equipment
(B) Glass particles

OD and 12-inch long cast acrylic tube with the 1/4-inch thick wall. Four holes, 1 1/2-inch in diameter, were drilled in the wall of the disengaging section 1 1/2-inches from the top to let the fluidizing air escape. These holes were covered with fine mesh screen to prevent the highly fluidized particles from being blown out of the column. One hole, inch in diameter, was made in the top plate which is covering the disengaging section, and that hole was occasionally used to put the particles into the bed and to blow out the unnecessary particles from the bed. An alumel-chromel thermocouple was inserted through the wall of the disengaging section to measure the air outlet temperature.

The Tube Bundle with the Heating Elements: The tube bundle is 60-inch long and consists of nineteen 321 stainless steel tubes 3/4-inch OD with 0.012-inch thick arranged in 1-inch triangular pitch. The complete tube layout is shown in Figure 7. The 3/16-inch stainless steel wire has been wrapped around the outside of each tube in a helical spiral. After examining the effect of the first wire as an extended surface, the second, the third, and the fourth wire was wrapped around each tube to see the gradual increase in wall-to-bed heat transfer. The details will be explained in Experimental Program. One end of each tube, except the

heating tubes, was fitted with a plastic plug to faciliate fitting into the lower tube sheet.

The heating tubes (4 tubes as shown in Figure 8) are fitted with copper electrodes on the top and the bottom. The top electrode has a porcelain tube inserted in it to prevent contact between the electrode and the aluminum tube housing the leads inside the heating tube. The bottom electrode is faciliated to fit into the lower tube sheet and has a 1/4-inch hole to accept a No. 10 copper wire used as a power lead.

The bottom tube sheet is made of a perforated steel sheet with a 200 mesh wire screen welded to it to prevent the moving particles from running out from the experimental section. The heating tubes are insulated from this sheet with rubber rings.

The Air Blower: Air was supplied by a Sutorbilt 57-TP air blower driven by a 1750 RPM, 7 1/2 HP AC induction motor. Two and one half inch steel pipe was used to transport the air to the experimental heat exchanger. The 2 1/2-inch pipe was reduced to two inches before entering the air intake section. The air flow rate was controlled by two gate valves. One, a two-inch-by-pass valve, controlled the air flowing through a by-pass to the atmosphere. The other control

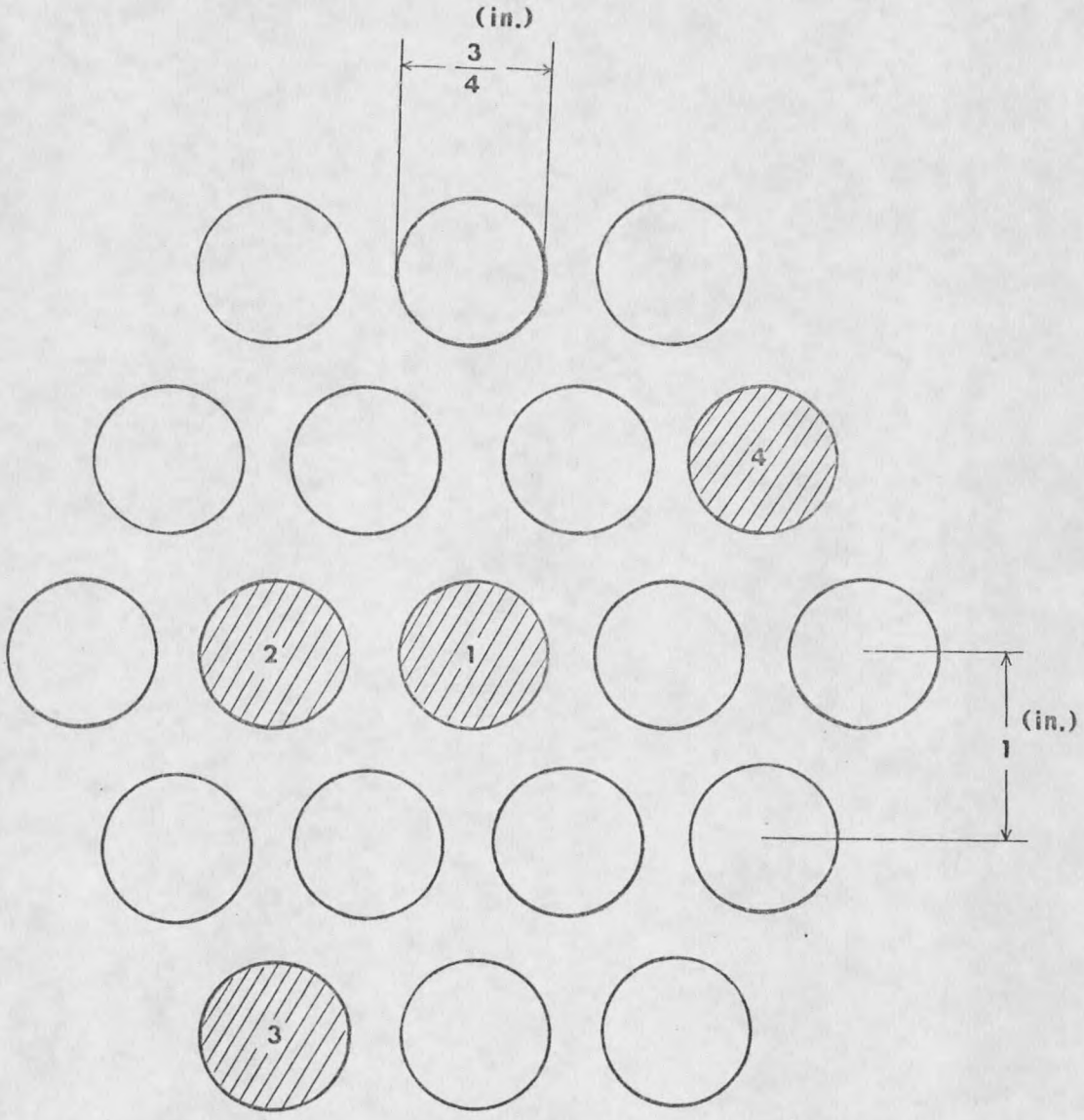


Figure 8. Tube layout: showing locations of heating element.

valve was in the 2 1/2-inch air supply line. The air flow was metered by a sharp-edged orifice located in the middle of the air supply line.

The Electric System and Power Source: A voltage transformer was used to supply energy to the wire wrapped stainless steel heating tubes. A diagram of the electrical circuit is shown in Figure 9. The resistance in the circuit was adjusted so that the current was about 48 amps. The emf and current were measured by an AC voltmeter with a range of zero to 15 volts and an AC ammeter with a range of zero to 50 amps.

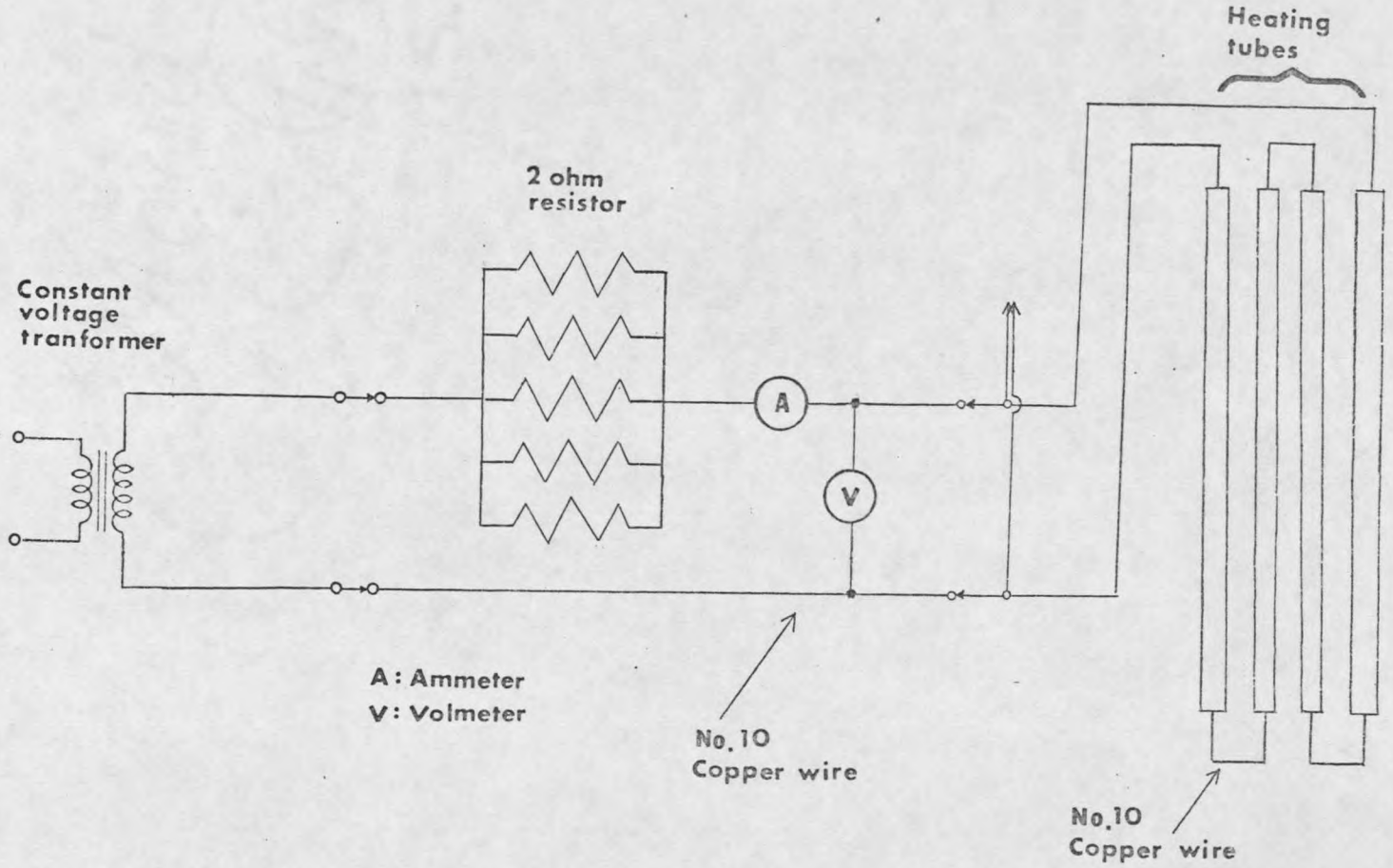


Figure 9. Diagram of electrical circuit.

Measuring Devices

Pressure: The U-tube manometers have been used to measure the pressure drop across the bed and an inclined (an angle of 30°) U-tube manometer has been used to measure the pressure drop across the sharp-edged orifice meter. A colored manometer fluid with a density of 1.00 gm/cm^3 was used.

Temperature: The wall temperature of the heating tubes (4 tubes as shown in Figure 8) were measured using chromel-alumel thermocouples. The thermocouple probe was designed to move up and down the heating tube. In this manner wall temperatures at various positions inside the tube wall were measured. Two insulated thermocouples were run through the probe casing which rounded to the shape of the tube wall, and both were embedded in two copper contact. Each copper contact was held against the inside tube wall with a spring.

The probe assembly is shown in Figure 10. As previously mentioned, eleven iron-constantan thermocouples were inserted through the wall of the experimental column to measure the bed temperatures. An iron-constantan thermocouple was placed inside the air distributing section and a chromel-alumel thermocouple was put into the middle of

the disengagin section. Both were to measure the gas inlet and outlet temperature. All reference junctions were kept in an ice bath at 32°F. The thermocouple emf was read using a Leeds and Northrup Co. potentiometer model 0381600. A switching system was used to complete the thermocouple circuits.

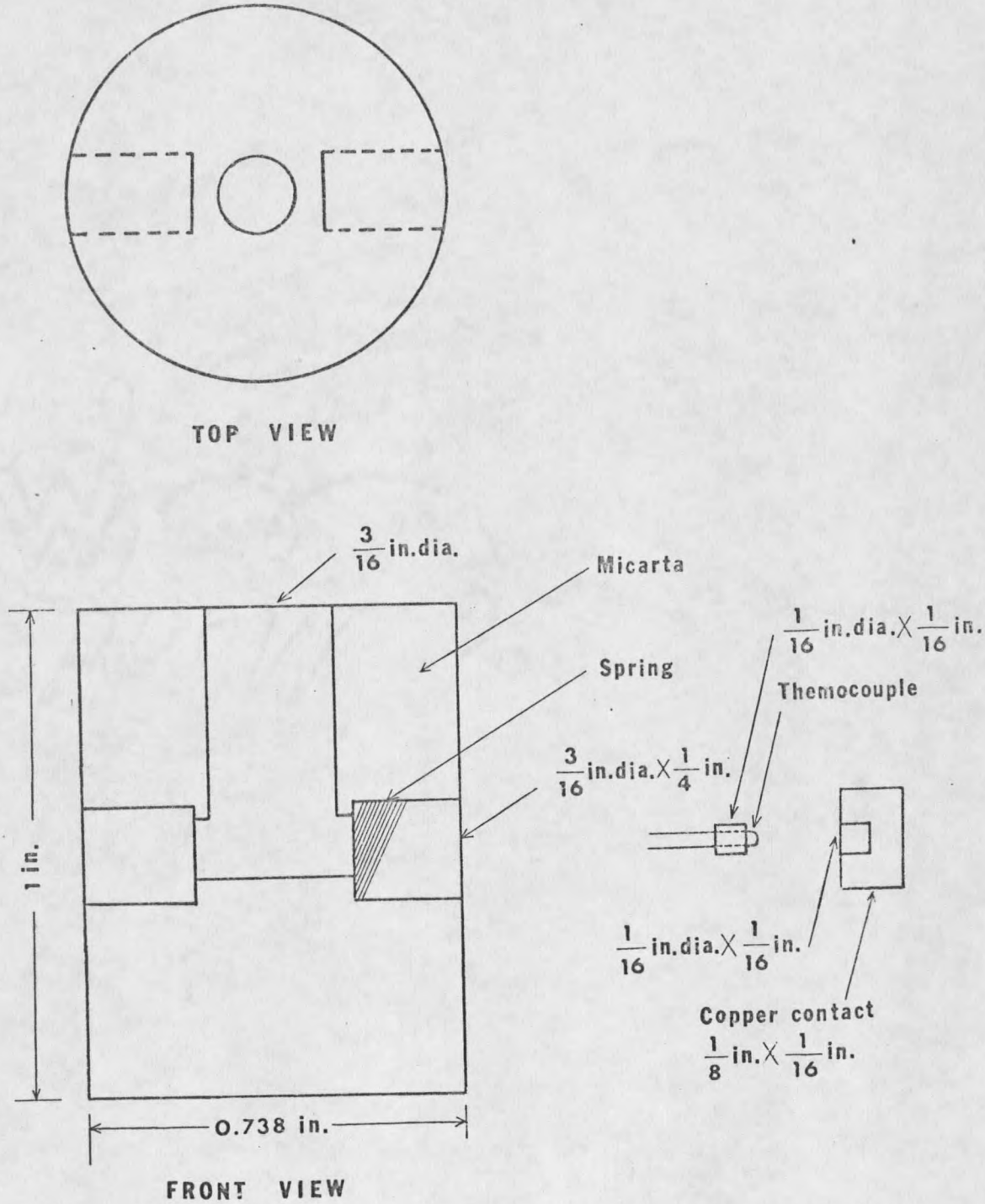


Figure 10. Exploded view of the tube wall temperature probe.

Experimental Program and Procedure

Experimental Program: The objective of this study is to determine heat transfer coefficients in a vertically arranged finned tube bundle for air flowing through a fluidized bed at various operating conditions. The stainless steel wires wrapped around the outside of each tube in a helical spiral have been used to increase the rate of heat transfer.

The variables to be considered in bed-to-wall heat transfer in gas-solid fluidized beds are: (1) properties of gas; density, ρ_g; viscosity, μ; specific heat, C_{pg}; thermal conductivity, k_g (2) properties of the solids: diameter, d_p; density, ρ_s; spherity, ϕ_s; specific heat, C_{ps}; (3) conditions at minimum fluidization: minimum fluidization velocity, u_{mf}; voidage, ε_{mf} (4) flow conditions: superficial velocity, u_o; void fraction, ε_f and (5) geometric properties: bed diameter, static bed height, the length of heat transfer surface, type of fin, and heating tube location.

Variables under consideration in this study are static bed height superficial gas velocity, heating tube location, and the extended surface area.

Heat flux, tube wall temperature profile, and vertical bulk gas temperature profile have been measured in order to

calculate the rate of heat transfer and to find out the effect of the increasing surface area.

Air has been used as the fluidizing medium and only one tube bundle configuration has been considered. The 3/16-inch stainless steel wire has been used as an extended surface.

Properties of Solids: Only one type and one size of solid particle has been used in this study. Coarse glass spheres, manufactured by 3M Company, of 0.0185-inch average diameter were used. The density of glass particles is 156 lb/ft^3. A microphotograph of the particles (Figure 8B) shows that the glass particles are spherical.

Static Bed Heights: Static bed heights of five, seven and nine inches have been investigated. Data were also taken without particles in order to compare with data reported by Donohue (6) and Genetti (8). Static bed heights were measured with a scale which was on the experimental heat exchanger column.

Fluid Mass Velocity: A wide range of gas velocities was used in this study to determine the most effective velocity and to find the effectiveness of extended surfaces as a function of gas flow rates.

Heating Tube Location: Since vertically arranged

finned tube layout is symmetrical as it is shown in Figure 8 only four heating tube locations were needed to investigate all possible heating tube locations. The rate of heat transfer has been studied at all four different locations for various static bed heights, gas velocities and the increasing ammount of extended surface (wrapped stainless steel wires). The heating tube locations are shown in Figure 8, and will be referred by number. The center location is numbered one; the location half the distance from the center is numbered two and the two outer locations are numbered three and four.

The heating tube wall tube temperature was measured at eleven positions along the tube. For all runs the locations were 1 1/2. 3 1/2, 7 1/2, 11 1/2, 15 1/2, 19 1/2, 23 1/2, 27 1/2, 31 1/2, 35 1/2 and 39 1/2 inches from the bottom were used to get the necessary data to obtain the temperature profile along the tube. These eleven positions are corresponding positions of the thermocouples which were inserted through the wall of the experimental column to measure the temperatures of the bed.

The Type of Fin: The 3/16-inch stainless steel wire has been used as an extended surface. The stainless steel wire has been wrapped around the outside of each 19 tubes

in a helical spiral.

After examining the first wire as an extended surface, the second, the third, and the fourth wire was wrapped around each tube to see the gradual wall-to-bed heat transfer increase with the increasing amount of extended surface. For the first wire, the rate of heat transfer were measured for different static bed heights and gas velocities at all different heating tube locations. The same procedure was used for the second, the third, and the fourth wire. The following chart shows the complete program of this study at different heating locations for various static bed heights, gas velocities and the increasing amount of extended surface.

Table I

No. of FBH	No. of Wire	SBH 5"	SBH 7"	SBH 9"
1	w1			
	w2			
	w3			
	w4			
2	w1			
	w2			
	w3			
	w4			
3	w1			
	w2			
	w3			
	w4			
4	w1			
	w2			
	w3			
	w4			

w1 = one extended surface w3 = three extended surfaces

w2 - two extended surfaces w4 = four extended surfaces

SBH = static bed height

FBH = fluidized bed height

1 = slightly fluidized (above minimum fluidization)

2 = fairly fluidized

3.= well fluidized

4 = highly fluidized

Experimental Procedure

The following routine procedure is followed before making each experimental run:

1. The desired amount of glass particles is placed in the experimental column. The air blower is turned on, and the control gate valves is adjusted to give the desired flow rate. The desired fluidized bed height is obtained by adjusting the correct openings for these two control valves. The valves are tightened to maintain the constant flow rate during the experimental period.

2. The power supply is turned on. The resistance in the electric circuit is adjusted so that the current will be about 46-50 amperes and the voltage about 7.8-8.6 volts.

3. A thermos flask is filled with crushed ice and water. The thermocouple reference junctions is placed in the flask to give a reference temperature of 32°F.

4. The potentiometer is balanced against an internal standard cell.

5. The tube wall probe thermocouples have been set to their initial positions.

6. When steady state has been observed in regard to tube wall temperature emfs, the recording of data is begun.

The following procedure has been used in recording the necessary data:

1. The voltage and current from the power supply are measured with an AC voltmeter and an AC ammeter. The pressure drop across the metering orifice is measured with a water manometer.

2. The tube wall probe thermocouple emf is measured with a potentiometer. The probe is then placed in the second position and the probe is allowed to attain steady state. The same procedure is continued until all 11 probe positions have been measured.

3. While the probe is coming to steady state between probe emf measurements, the remaining data are measured. The gas inlet temperature, gas outlet temperature, 11 bulk gas temperatures, and bed pressure drops are recorded at 11 equal time intervals during the course of the run.

4. The power supply voltage and current are checked again and averaged. The orifice pressure drop is also checked at the end of the run.

After all the data are recorded for one run, the equipment is turned off, or the procedure is repeated again for another fun. In this manner, data are taken for the different static bed heights, gas flow rates, and an in-

creasing amount of extended surface area at different heating tube locations. A typical data sheet can be found in Appendix III.

Calculations

The basic calculations are gas flow rate, temperature calculations from thermocouple emf's, local temperature differences, heat flux, local heat transfer coefficients, weighted local heat transfer coefficients, average heat transfer coefficient, and section pressure drops. From the above calculated data bed section void fractions and bed section average heat transfer coefficients have been calculated.

All calculations have been performed with the aid of SDS SIGMA 5/7 and HEWLETT-PACKARD 2116B digital computers. Softwares used are Basic, Fortran IV and APL. All of these are listed in Appendix IV.

Computations Using Readings:

The key emf values which bracket the temperature range measured for the local tube wall temperature and gas outlet temperature are 1.52, 1.98, 2.45, 2.89, 3.36, and 3.81. Passing a fifth-order polynomial through these six points gives the good fit over the temperature range. The calculated results have been compared with calibration tables for thermocouple chromel-alumel thermocouples in Appendix V. The key values which bracket the temperature range measured

for the local bulk fluidized bed temperature and gas inlet temperature are 1.65, 1.79, 1.94, 2.08, 2.23, 2.38, and 2.52. The form of the Lagrangian formula given by a sixth-order polynomial through these 7 points gives the good fit over the temperature range. The calculated results have been compared with calibration tables for iron-constantan thermocouples in Appendix V. Since the Lagrange's interpolation formula is applicable for either equal or unequal intervals, the interpolated functional value corresponding to any given E(x) is given by T.

The bulk fluidized bed temperatures are calculated for the 11 tube wall probe positions according to the numerical method described above, and then the local temperature difference is calculated from the following equation:

$$\Delta T_{loc} = T_w - T_b \tag{34}$$

The heat flux was calculated by determining the power dissipated in the heating element. The product of the measured current and voltage drop gives the power dissipated in the heating element and the connecting leads. The expression used for the heat flux the electrical resistance of the leads under consideration is:

$$Q = 0.87(I\ V - 0.03122\ I^2) \tag{35}$$

The local heat transfer coefficient is calculated from the following equation:

$$h_{loc} = Q/\Delta T_{loc} \tag{36}$$

The equation used to calculate the average heat transfer coefficient is as follows:

$$h_{av} = Q/\Delta T_{av} \tag{37}$$

where

$$\Delta T_{av} = \frac{1}{L} \int_0^L \Delta T_{loc} dZ$$

This integral has been numerically evaluated using a least-square polynomial fit of degree n.

The pressure drop across the sharp-edged orifice is measured with a manometer inclined at 30°. The pressure balance of the two columns in the inclined U-tube manometer gives

$$\Delta P_{orifice} = \frac{g}{g_c} \Delta h(\rho_L - \rho_g) \sin \frac{\pi}{6} \tag{38}$$

where Δh = the reading of manometer in feet.

The actual gas flow rate G is calculated from the sharp-edged orifice calibration. The generalized equation to calculate the mass flow rate through a constant-area differential type of fluid meter is

$$\dot{w} = KA_m Y[2\rho_{g1}(P_1-P_2)]^{1/2} \qquad (39)$$

$\dot{w}$ + actual mass flow

A_m = the cross sectional area of a flow meter, ft^2

ρ_{g1} = gas density upstream location, lb_m/ft^3

and for a compressible fluid the expansion factor, Y, is used and is given by

$$Y = 1 - (0.41 + 0.35\beta^4)\frac{P_1-P_2}{\gamma P_1} \qquad (40)$$

where β = the ratio of the diameters

$\gamma = C_p/C_v$

Kretzschmer (26) has shown that

$$K = \frac{C}{(1-\beta^4)^{1/2}} \qquad (41)$$

where C = coefficient of discharge, dimensionless. However, the equation which has been used to calculate the gas flow rate from the pressure drop across a concentric, sharp-edged orifice is

$$G = \frac{3600K\ YA_o}{A_h}[2g_c\Delta P_{orifice}\rho g1]^{1/2} \qquad (42)$$

where G = mass flow rate, $lb_m/hr\ ft^2$

A_o = cross sectional area of orifice opening, ft^2

A_h = cross sectional area of heat exchanger, ft^2

g_c = 32.174 $lb_f ft/lb_m sec^2$

The pressure drop across the fluidized bed over 11 different positions are measured with manometers using a manometer fluid having a specific gravity of 1.00. The following equation gives this pressure drop:

$$\Delta P_b = \frac{g}{g_c} \Delta h \, (\rho_L - \rho_g) \qquad (43)$$

where Δh = the manometer reading in ft.

Computations From the Calculated Data:

The void fractions, ε, are calculated for each of 11 positions, where pressure taps are located, of the heat exchanger from the measured values of bed section pressure drops. The following equation is a good approximation for batch fluidization:

$$1-\varepsilon = \frac{\Delta P_b \, g_c}{L_g \, \Delta \rho} \qquad (44)$$

The minimum fluidization mass velocity is calculated using the following equation (21):

$$G_{mf} = \frac{0.00125 \, D_p^{\,2} (\rho_s - \rho_g)^{0.9} \rho_g^{\,1.1} \, g}{\mu} \qquad (45)$$

Analysis of Data

Average Nusselt Numbers Correlation Without Fluidization

Data were taken without fluidization to compare the resulting average Nusselt numbers with the following correlation:

$$\frac{h_{av}}{k_g} = C_0 D_e^{0.6} \left(\frac{deG}{\mu}\right)^{0.6} Pr^{1/3} \qquad (46)$$

where D_e = the equivalent diameter in inches based on four times the hydraulic radius.

The term $\left(\frac{h_{av}}{k_g}\right)\left(P_r^{-1/3}\right)$ was calculated from the data with $P_r = 7.05$ in all cases. This dimensionless product is plotted versus the dimensional term $D_e \frac{d_t G}{\mu}$ in Figure 11. The correlation of Genetti (8) is also represented in Figure 11. The correlation of Genetti (8) is within +25 percent of Donohue's correlation (6).

Calculated Nusselt numbers using equation 46 are all higher than those calculated from Genetti (8) and Donohue (6). This is what would be expected since extended surface area for heat transfer is available. The solid line shows Genetti's results for a bare bundle with 3/4-inch tubes.

Vertical Fluidized Bed Temperature Profiles

With the aid of 11 thermocouples protruding from the

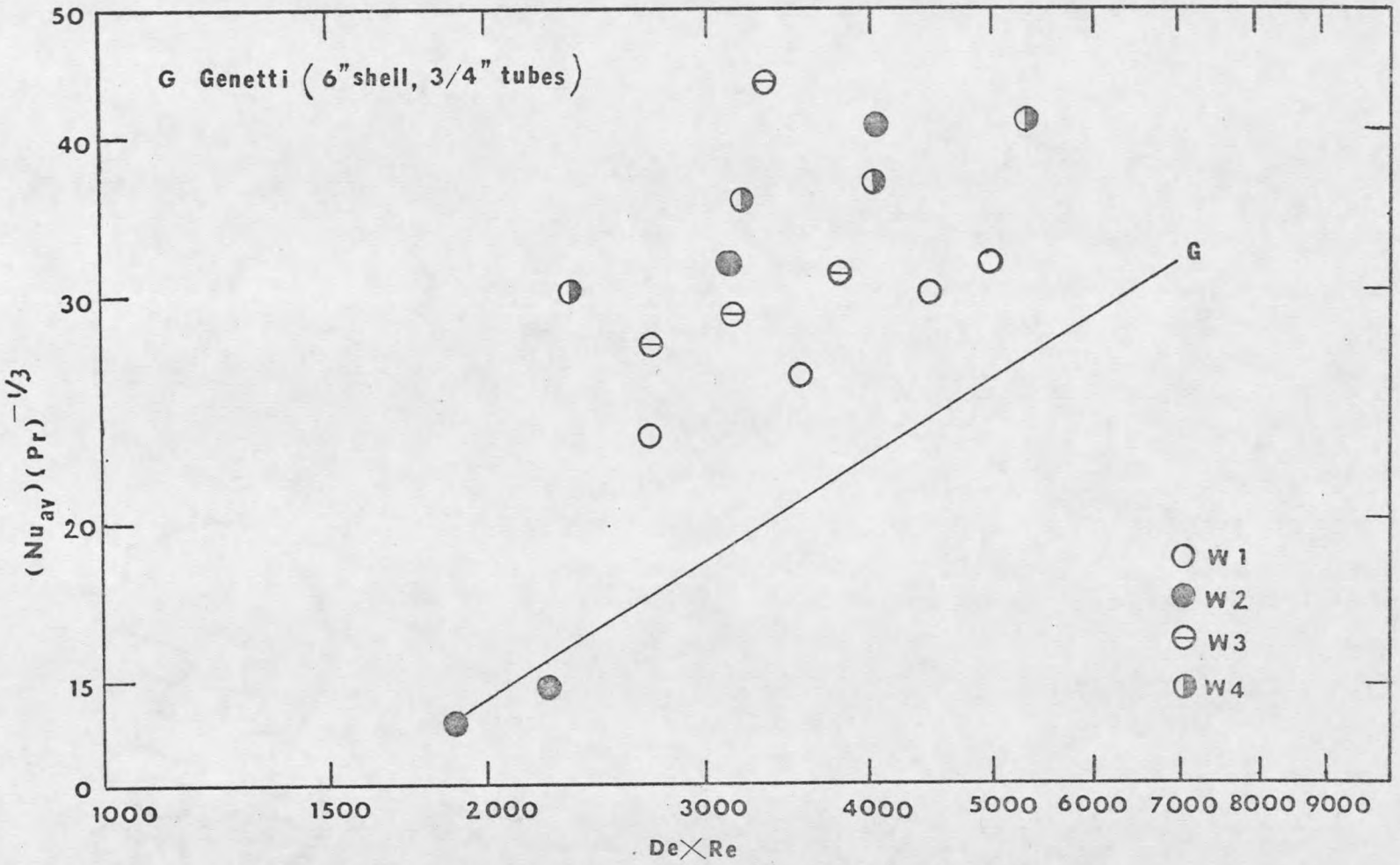


Figure 11. Average Nusselt numbers correlation with fluidization.

outer wall of vertical column, fluidized bed temperatures were determined. Static bed height of seven inches and nine inches were examined. Vertical bulk gas temperature profiles for well fluidized beds are shown in Figure 12. For the uses shown mass velocities are approximately same. Two different amount of extended surfaces were compared.

Figure 12 (A) and (B) are static bed heights of seven inches and nine inches respectively and for the first extended surface. Figure 12 (C) and (D) are also for static bed heights of seven and nine inches, but with four times the extended surface area. All profiles show a uniformly distributed temperature profile; however, for greater extended surface area this effect is more noticeable. For static bed height of seven inches the fluidization height was approximately 31 inches, and for nine inches the fluidization heights were around 38-42 inches.

Local Heat Transfer Coefficients for Batch Fluidization

Local heat transfer coefficients are plotted versus the probe number from the experiemntal tube entrance of a constant gas mass velocity. The weighted average local heat transfer coefficients of four different tube locations have been calculated for each run. This weighted average local heat transfer coefficients of one extended surface

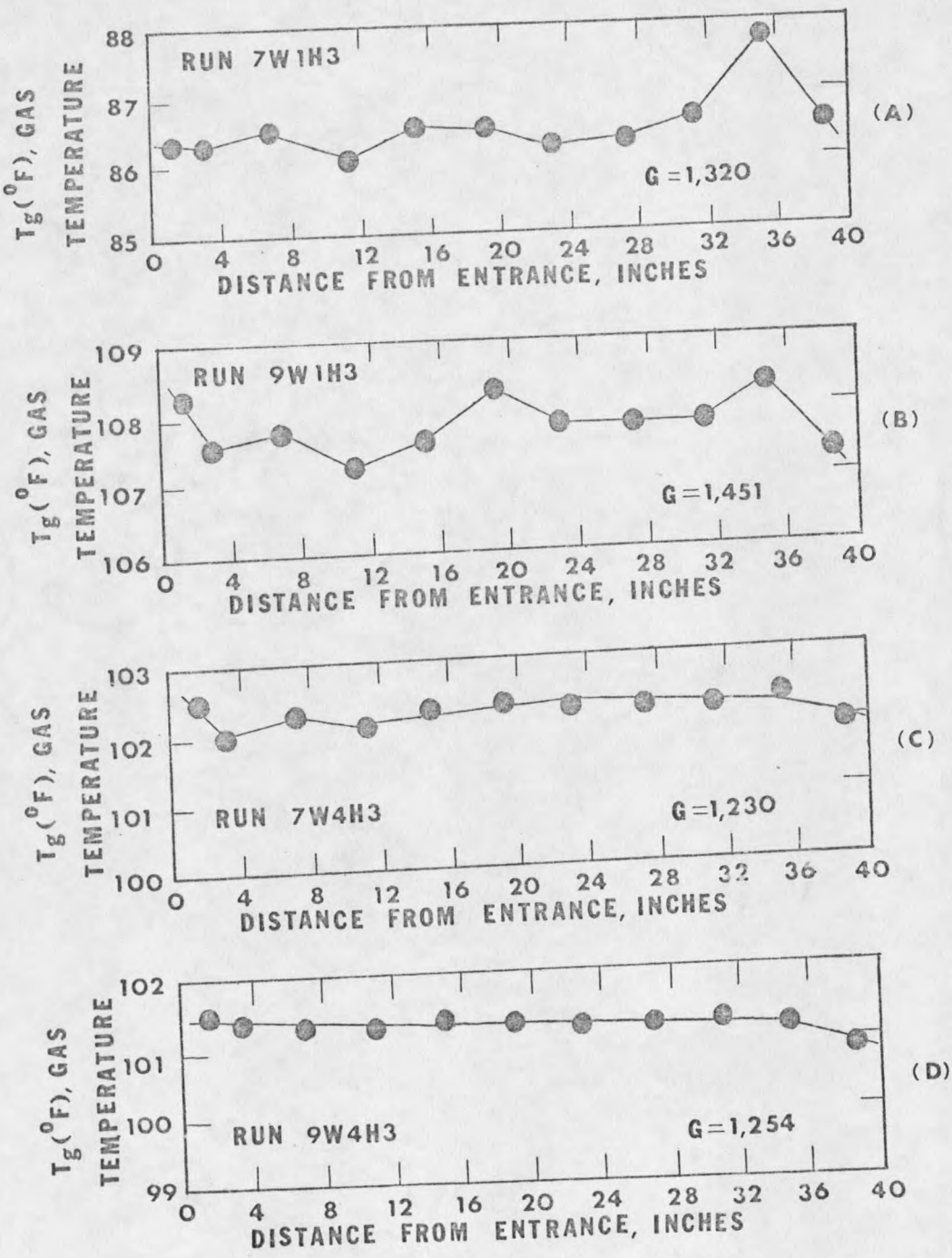


Figure 12. Vertical fluidized bed temperature profiles.

are compared to the average local heat transfer coefficients of two, three and four extended surfaces to observe the effect of the increasing amount of the extended surface. Wire 1 indicates one extended surface. Wire 2 indicates one more added, therefore, two extended surfaces and so on.

Approximately the same static bed height, fluidized bed heights, and gas mass velocities were used to assure the same conditions for four different extended surface areas considered.

Figure 13 shows local heat transfer coefficients for the slightly (just a little bit above the minimum fluidization) fluidized bed. The data are for static bed height of five inches and mass velocities of 526 and 481 $lb_m/hr\ ft^2$. For these mass velocities particles were fluidized to the heights of approximately eight and nine inches. Above these heights the amount of extended surface had no significant effect on local heat transfer coefficients.

Since the fluidized bed heights were around eight and nine inches, the weighted average coefficients for probe one, probe two, probe three, and probe four have been compared. Profiles of Wire 1 and Wire 2 show that the coefficients of Wire 2 are slightly higher than Wire 1. Profiles of Wire 3 and Wire 4 also show that the coefficients of Wire 4 are slightly higher than Wire 3 and both are relatively higher

than the coefficients of Wire 1 and Wire 2. Coefficients are lower in these cases than for runs at higher mass velocities, and a rapid drop in heat transfer coefficients is observed at the position above probe 4.

The highly fluidized bed for static bed of five inches is shown in Figure 14. The data are for mass velocities of 1442, 1458, 1410, and 1360 $lb_m hr\ ft^2$ respectively. The overall length of the test section was 44 inches, and in this series of runs particles were fluidized to the heights of approximately 33 and 38 inches. These are the most highly fluidized condition for static bed of five inches in this investigation. Gradual increase in the weighted average coefficients with respect to the number of extended surface is observed. Comparing the heat transfer coefficients, local heat transfer coefficients of Wire 4 are remarkably higher than the other. For Wire 1, Wire 2, and Wire 3 the coefficients are slightly increasing with the number of wires. In the lower part of the fluidized bed significant increase in local heat transfer coefficients is observed for Wire 1, Wire 2, and Wire 3. In the higher section of the Figure the amount of increase on local heat transfer coefficients of Wire 4 compare to Wire 3 was 29-38 $Btu/hr\ ft^2{}^\circ F$. Gradual decrease in local heat transfer coefficients with distance

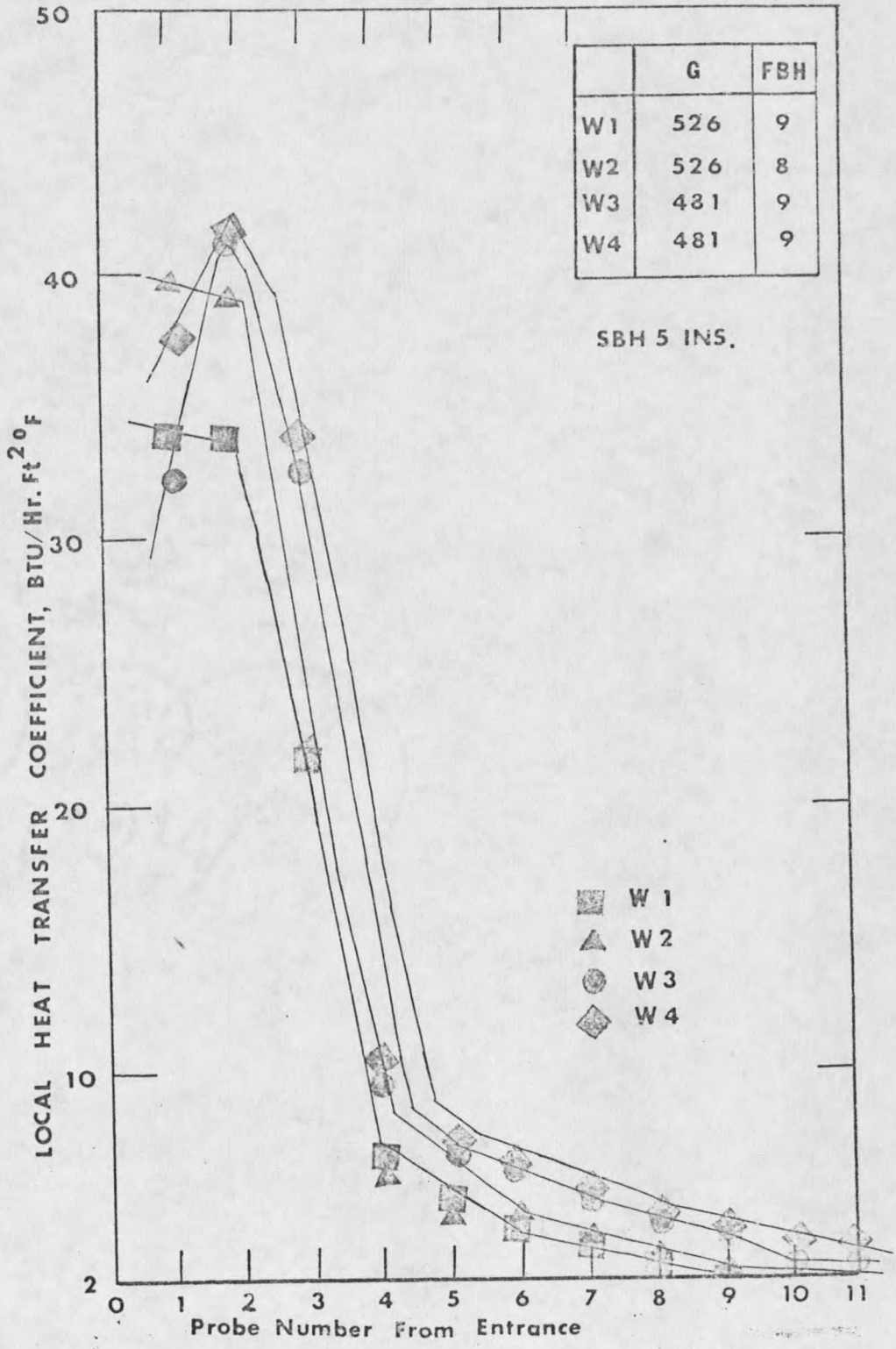


Figure 13. Local heat transfer coefficients.

is observed. In the lower part of the fluidized bed the particle concentration is greater than the higher section and it causes the higher heat transfer rate. For static bed height of five inches local heat transfer coefficient profiles are of Type I, as described by Toomy and Johnstone (27). For relatively low static bed height it has been observed that local heat transfer profiles are of Type I. This agrees with Genetti (8). Genetti has also investigated that heat transfer coefficient profiles for static bed height of four inches were of Type I except for the coefficient profile at tube location 2.

The well fluidized bed for static bed height of seven inches is shown in Figure 15. The data are for mass velocities of 1335, 1238, and 1235 $lb_m/hr\ ft^2$. For these mass velocities particles were fluidized to the heights of around 30 inches. Gradual increase in the weighted average coefficients with respect to the number of increased extended surface is observed. In the lower part of the fluidized bed where particle concentrations are high ($1-\varepsilon = 0.1 \sim 0.3$) the increase of local heat transfer coefficients with the increasing amount of extended surface was observable. For instance, in probe 3 local heat transfer coefficients for Wire 1, Wire 2, Wire 3 and Wire 4 were 36.43, 39.22, 40.43, and 45.23 respectively. The same tendency was observed up till probe 8.

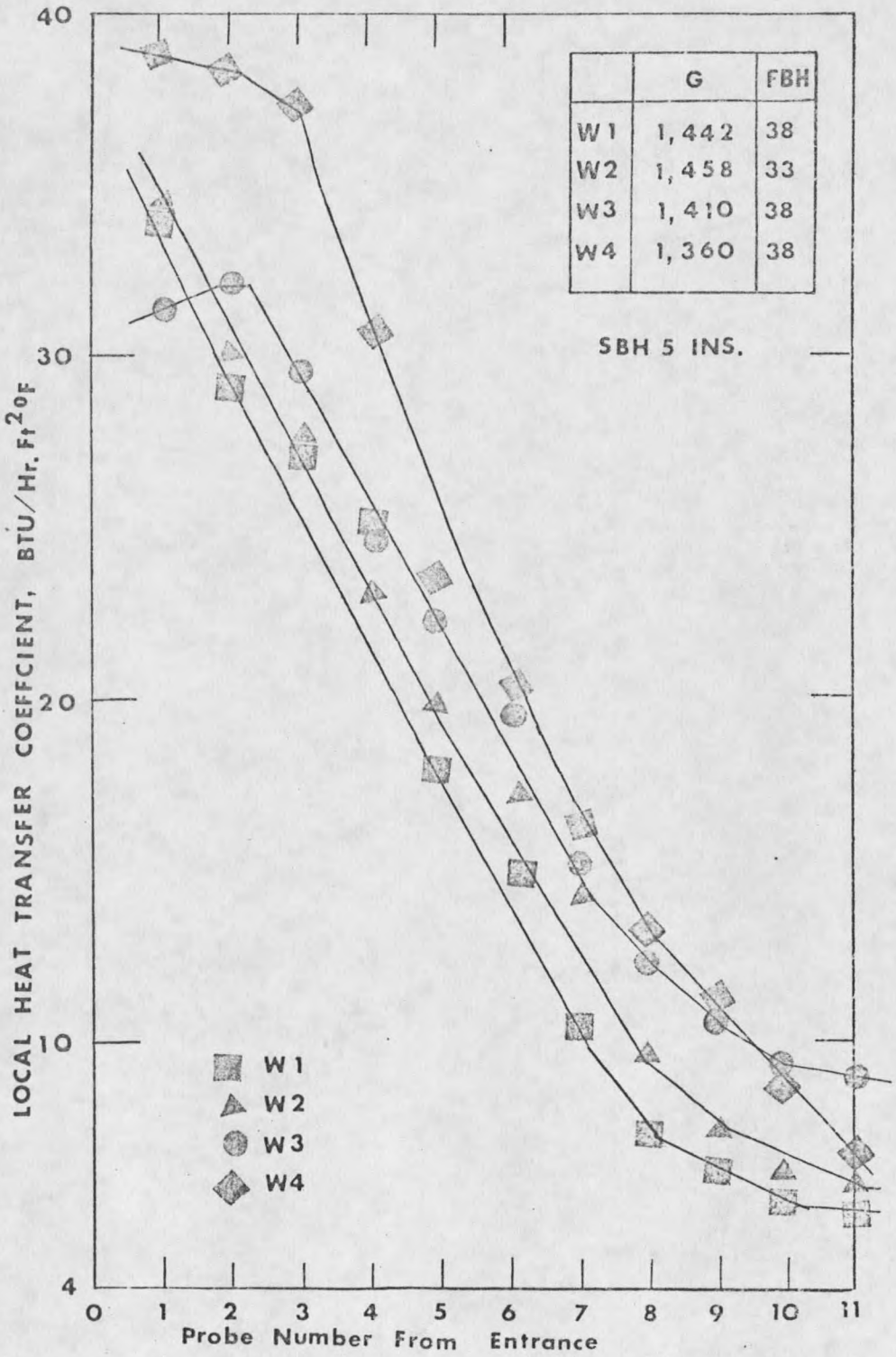


Figure 14. Local heat transfer coefficients.

For Wire 1 and Wire 2 profiles are of Type I. Toomey and Johnstone (27) concluded that in the study curves of Type I prevailed in all runs in which the dimensionless group $d_p L_f/A_T$ was greater than 0.008. However, the profiles of Wire 3 and Wire 4 are of Type II while the value of the dimensionless group $d_p L_f/A_T$ is 0.0091. The general flow pattern within the system apparently determines the shape of the curve. With this in mind the dimensionless group $d_p L_f/A_T$ is too simple representation to determine the shape of curve.

For G = 1490, the entire experimental column was fluidized for static bed height of seven inches. Figure 16 shows these runs. Particularly, significant increase in local heat transfer coefficients for Wire 4 in the dense part of the bed was observed. At probe 4 heat transfer coefficients seem somewhat inconsistent since the magnitude of increase in the coefficients for Wire 2 and Wire 3 is supposed to be larger than Wire 1, and yet the coefficients of those are lower than Wire 1. Heat transfer profiles for these runs are of Type I.

Figure 17, Figure 18 and Figure 19 are of static bed height of nine inches. Observable increase in local heat transfer coefficient with respect to the extended surface

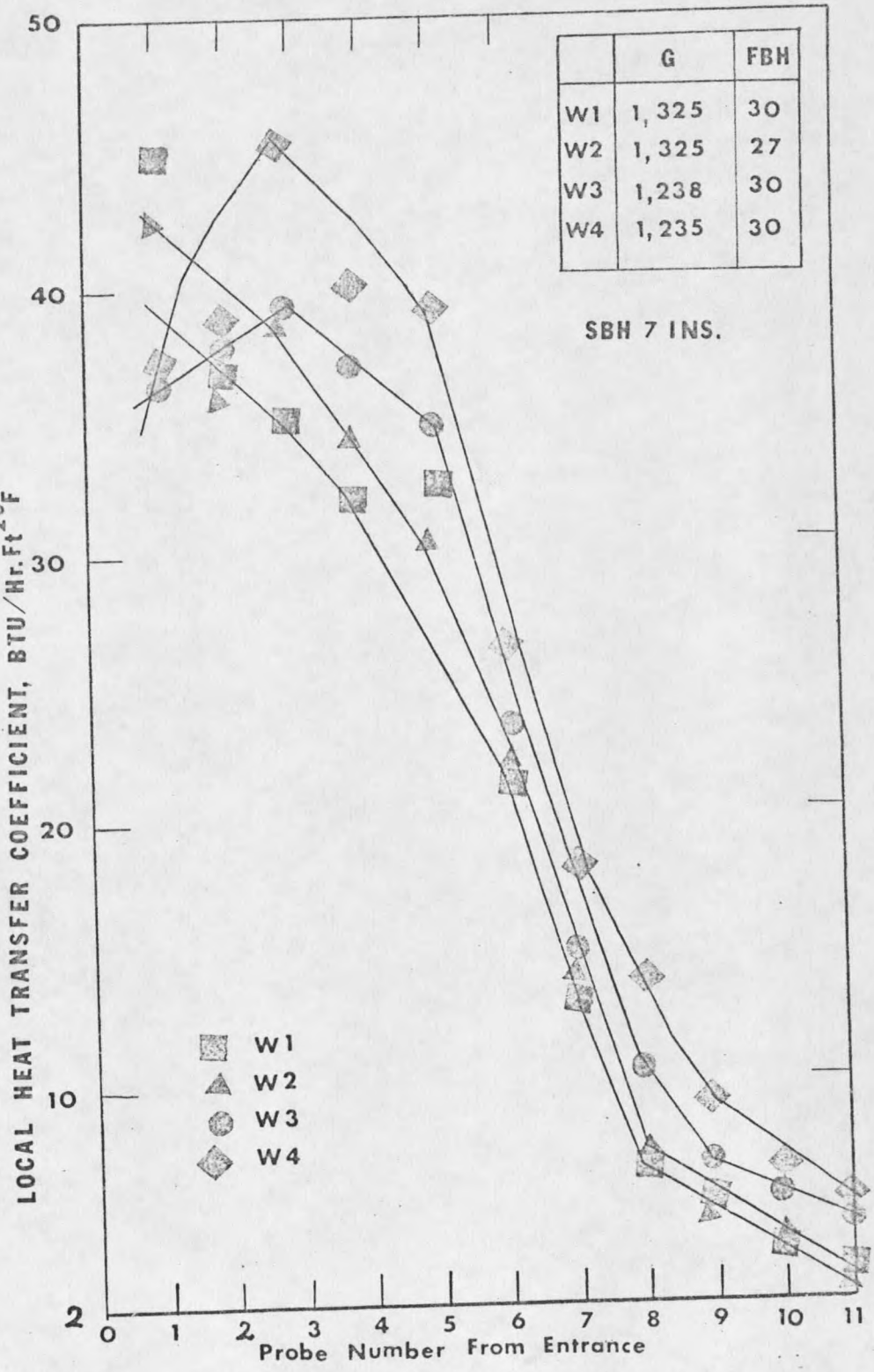


Figure 15. Local heat transfer coefficients.

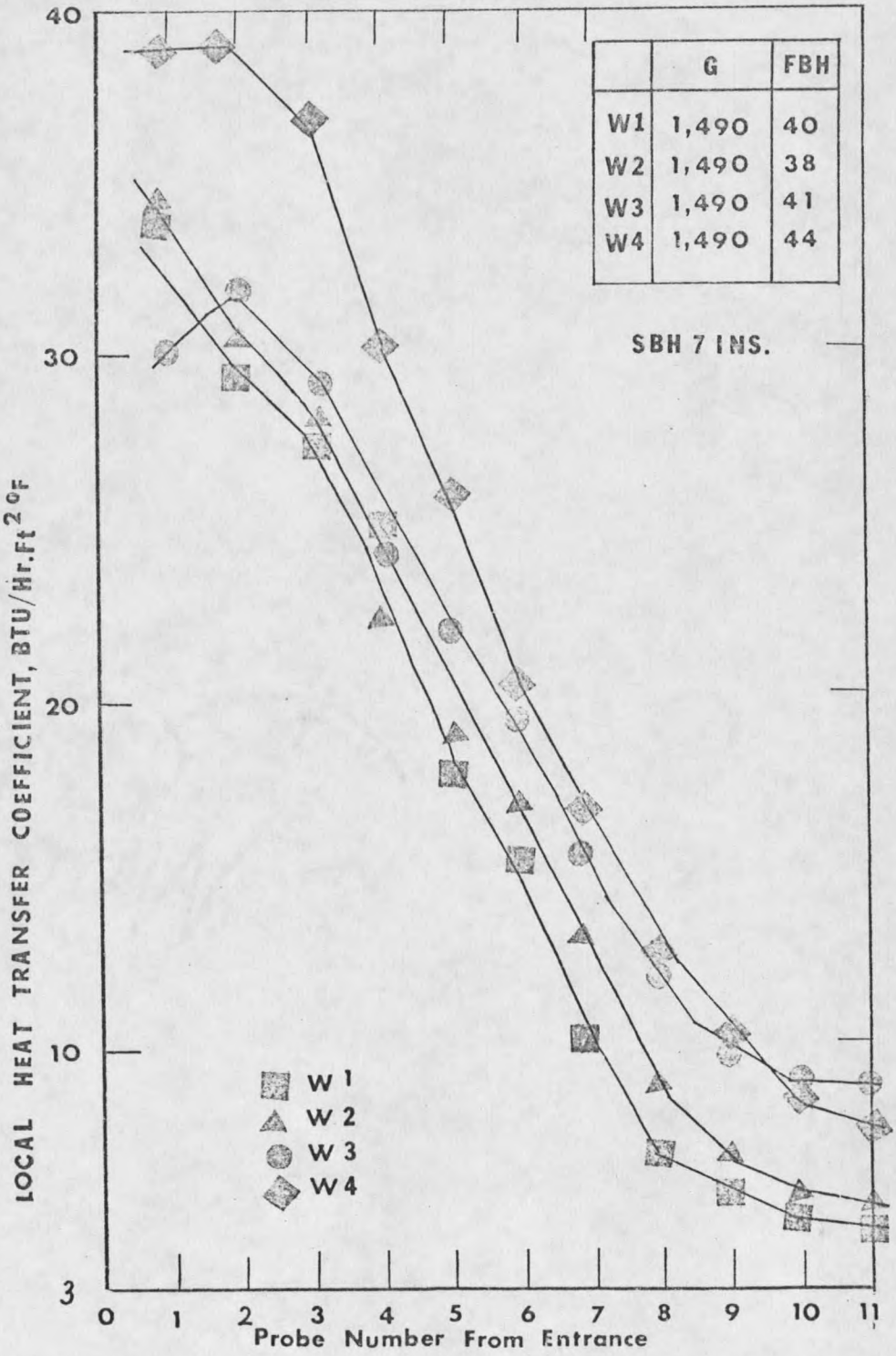


Figure 16. Local heat transfer coefficients.

area was observed. For static bed height of nine inches the difference of the coefficient between Wire 1, Wire 2, Wire 3 and Wire 4 were remarkably large compared to static bed height of five and seven inches.

Table II

Difference of Local Heat Transfer Coefficient Between Different Extended Surface

Extended Surface	Local Heat Transfer Coefficient Btu/hr ft^2°F			
	Probe 2	Probe 3	Probe 4	Probe 5
Wire 1	37.69	36.34	29.33	18.54
Wire 2	40.16	40.03	36.67	21.14
Wire 3	62.45	67.45	62.34	59.81
Wire 4	66.91	81.13	77.58	76.98

Table II shows the difference of heat transfer coefficient between different extended surface for mass velocities of 745 and 886 $lb_m/hr\ ft^2$. For this particular run particles are fluidized to heights of approximately 18 to 21 inches. Local heat transfer coefficients were high while in the dense part of the fluidized bed $1-\varepsilon$ was around 0.3. The profiles of Wire 1 and Wire 2 are of Type I.

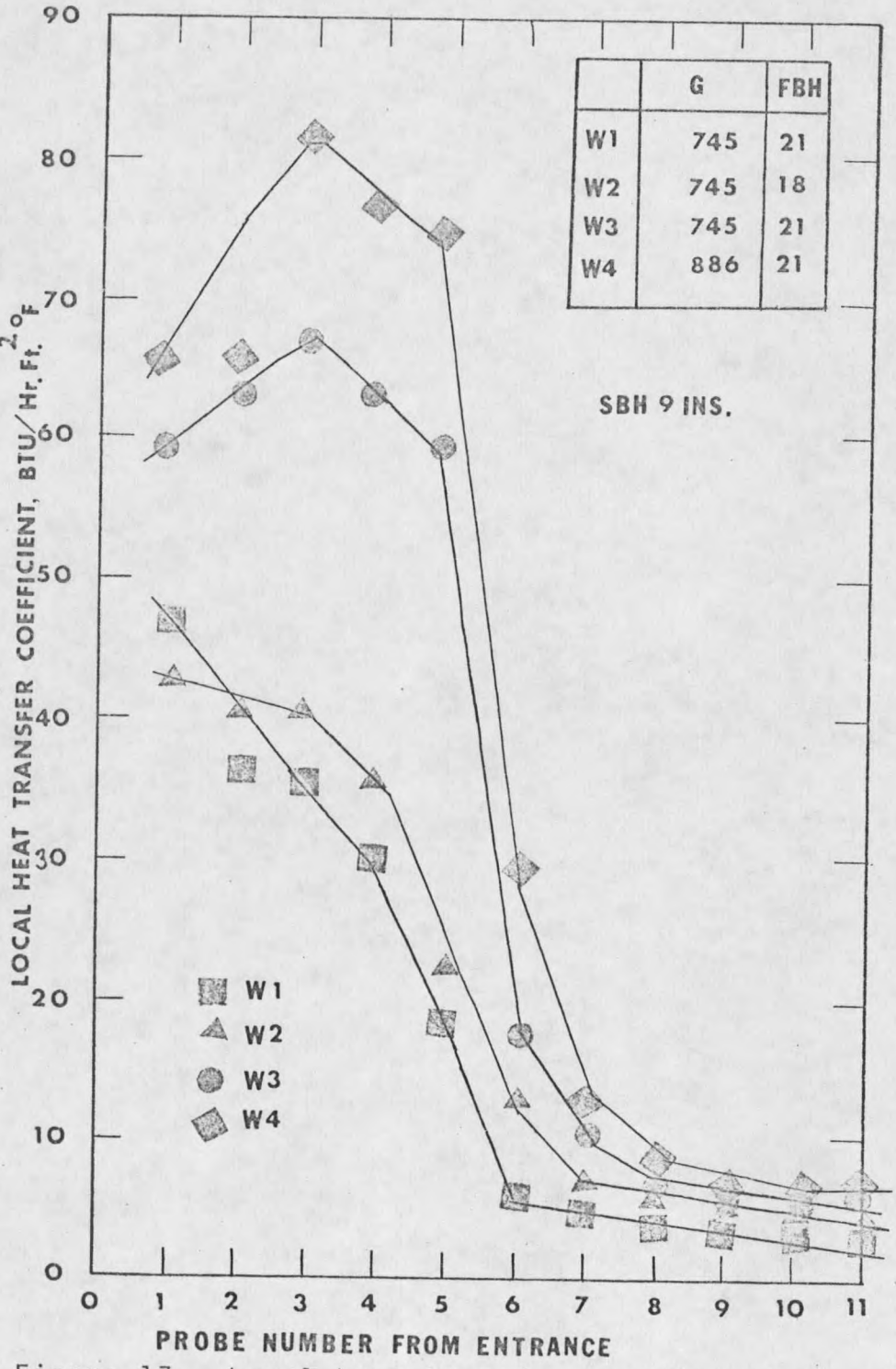


Figure 17. Local heat transfer coefficients.

In Figure 18 particles were fluidized to heights of 24 to 29 inches. If we consider up to probe 8 in these runs, the profiles all are of Type II while the value of the dimensionless group $d_p L_f / A_T$ is well over 0.008 (approximately 0.108). The profiles of Wire 3 and Wire 4 in Figure 17 are also of Type II. Genetti (8) has indicated that increases in the magnitude of the group, $D_t^2 / L_f S_b$, appear to increase the tendency toward Type II profiles. For static bed height of nine inches and in Figure 19 the group $D_t^2 / L_f S_b$ is about 0.0025. This agrees with Genetti (8) since the percentage of Type I profiles was 20 percent, when the value of the goup $D_t^2 / L_f S_b$ is 0.0306.

In Figure 19 the difference of local heat transfer coefficients between Wire 1, Wire 2, Wire 3, and Wire 4 are evidently comparable at each probe. Gradual decrease in local heat transfer coefficients with distance is observed. Relatively low coefficients for Wire 1 are observed.

The highly fluidized bed for static bed height of nine inches is shown in Figure 20. The entire section of the experimental column was fluidized. Mass velocities of 1665, 1693, 1637 and 1506 $lb_m/hr\ ft^2$ were examined. For Wire 4 local heat transfer coefficients are lower than Wire 3. However, the uniform temperature difference from

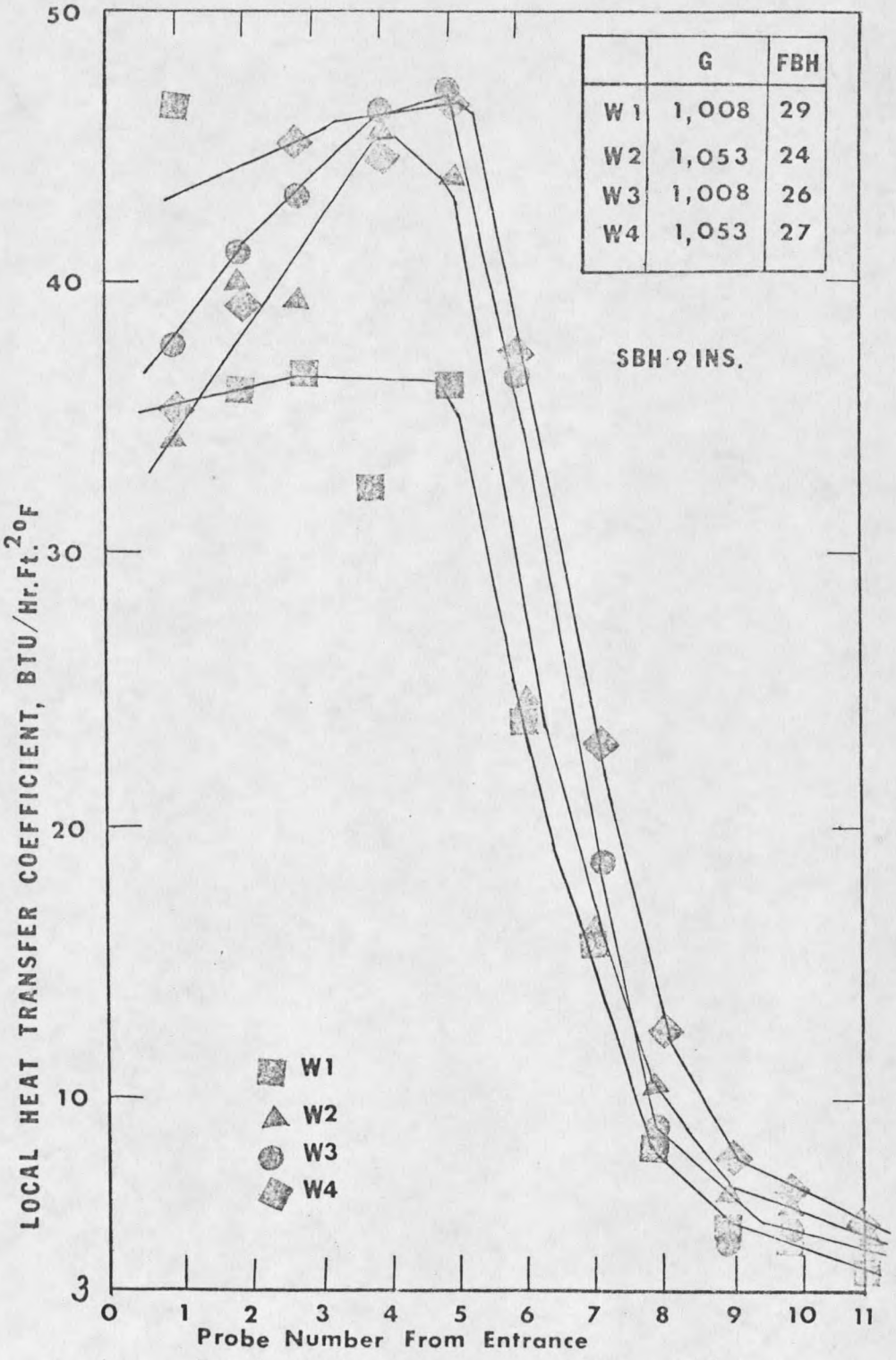


Figure 18. Local heat transfer coefficients.

probe 1 to probe 6 (local heat transfer coefficients are around 35 Btu/hr ft^2°F) were observed. Gradual decrease in local heat transfer coefficients with distance is also observed.

Figure 20 and Figure 21 are typical in the case of the well-fluidized bed. Vertical fluidized gas temperatures are uniform and the temperature difference between the fluidized bed and the heating wall throughout the bed are gradually increasing with the small magnitude. With the increased amount of extended surfaces this effect was particularly noticeable. Therefore, local heat transfer coefficients were increasing gradually with the increased amount of extended surfaces.

The Dependency on Tube Locations

No significant dependency on tube location has been observed. However, in low static bed height and in low mass velocities, wall temperatures vary slightly from tube to tube., with no consistent trend. At high static bed heights and at high mass velocities negligible difference in wall temperatures between different tube locations has been noticed.

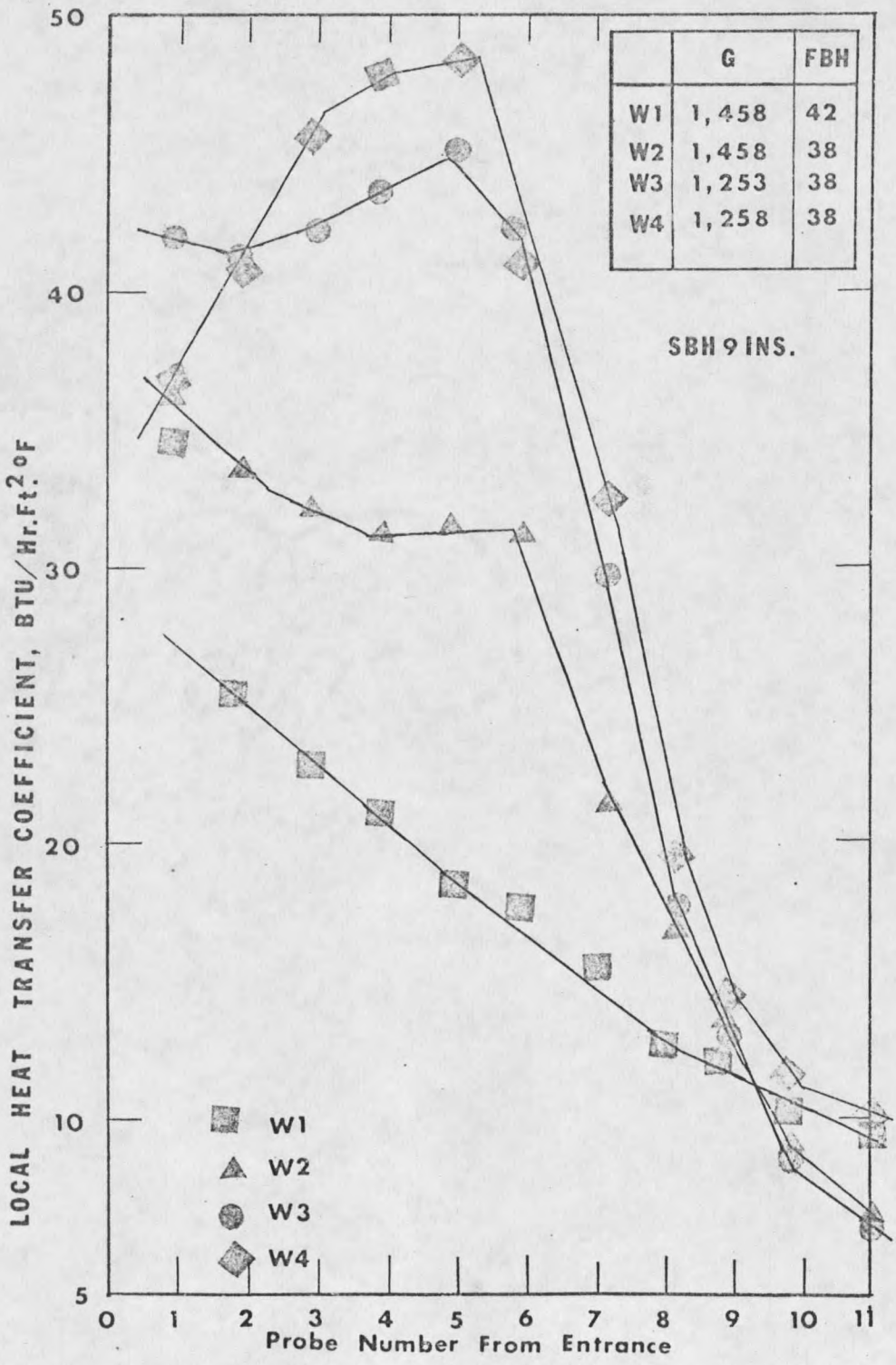


Figure 19. Local heat transfer coefficients.

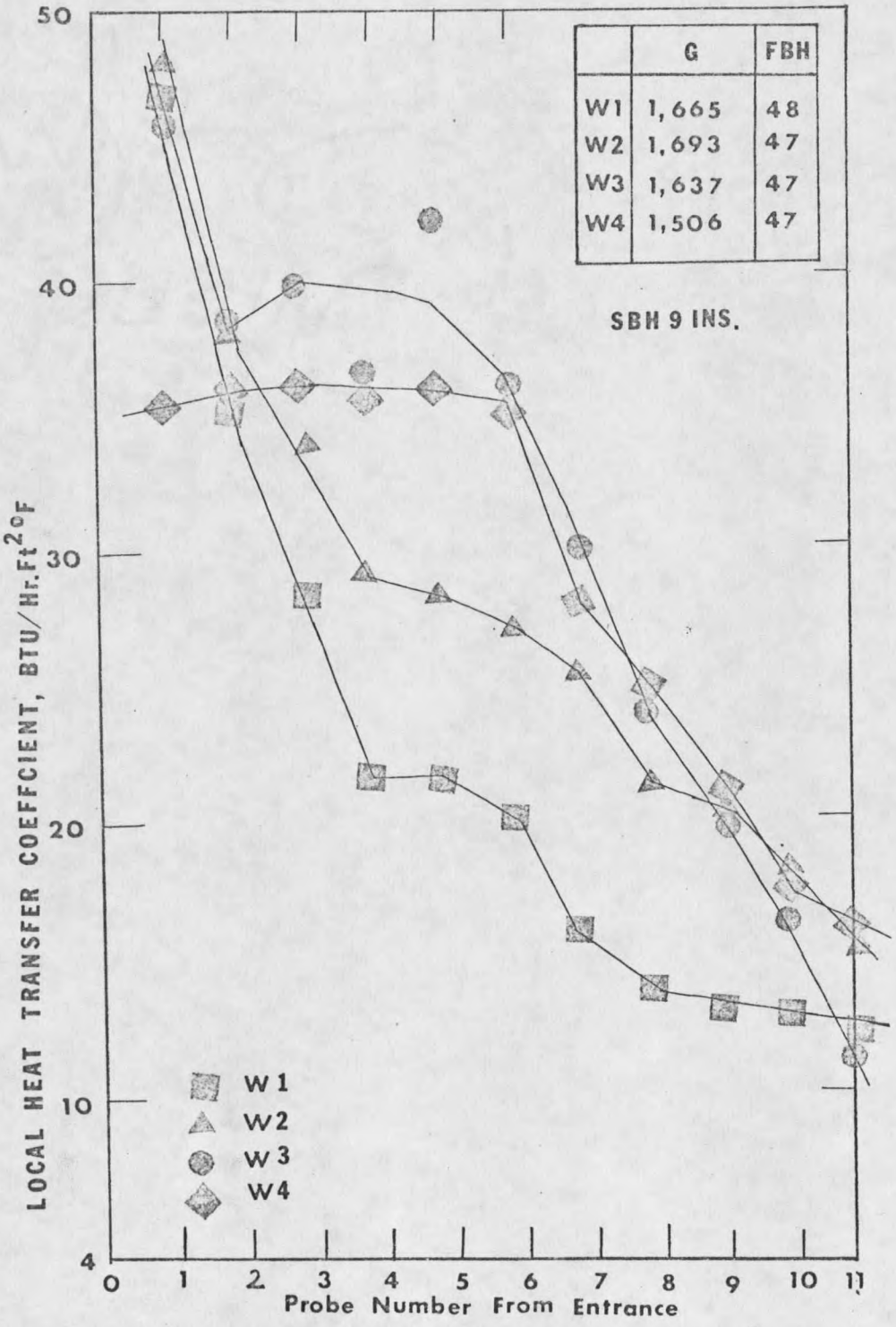


Figure 20. Local heat transfer coefficients.

Average Sectional Coefficients for Batch Fluidization Genetti's Correlation

Equation 30, the correlation for average Nusselt numbers, is shown in Figure 21. The calculated data for static bed height of nine inches using Equation 30 are also shown in Figure 21.

With experimentally determined sectional particle fractions and local heat transfer coefficients over 11 different sections of the fluidized bed average sectional coefficients for Wire 1, Wire 2, Wire 3, and Wire 4 are compared.

None of the data calculated using Equation 30 is below Genetti's data. Noticeable increase in average sectional coefficients with respect to extended surface area is noticed. The least square fits of the data for each extended surface show that the exponent for $1-\varepsilon$ range from 0.46 to 0.52.

One of the variables to be considered in bed-to-wall heat transfer is geometric properties of extended surface on average sectional coefficients should be determined. This variable should also correlate with the expression of average sectional coefficients.

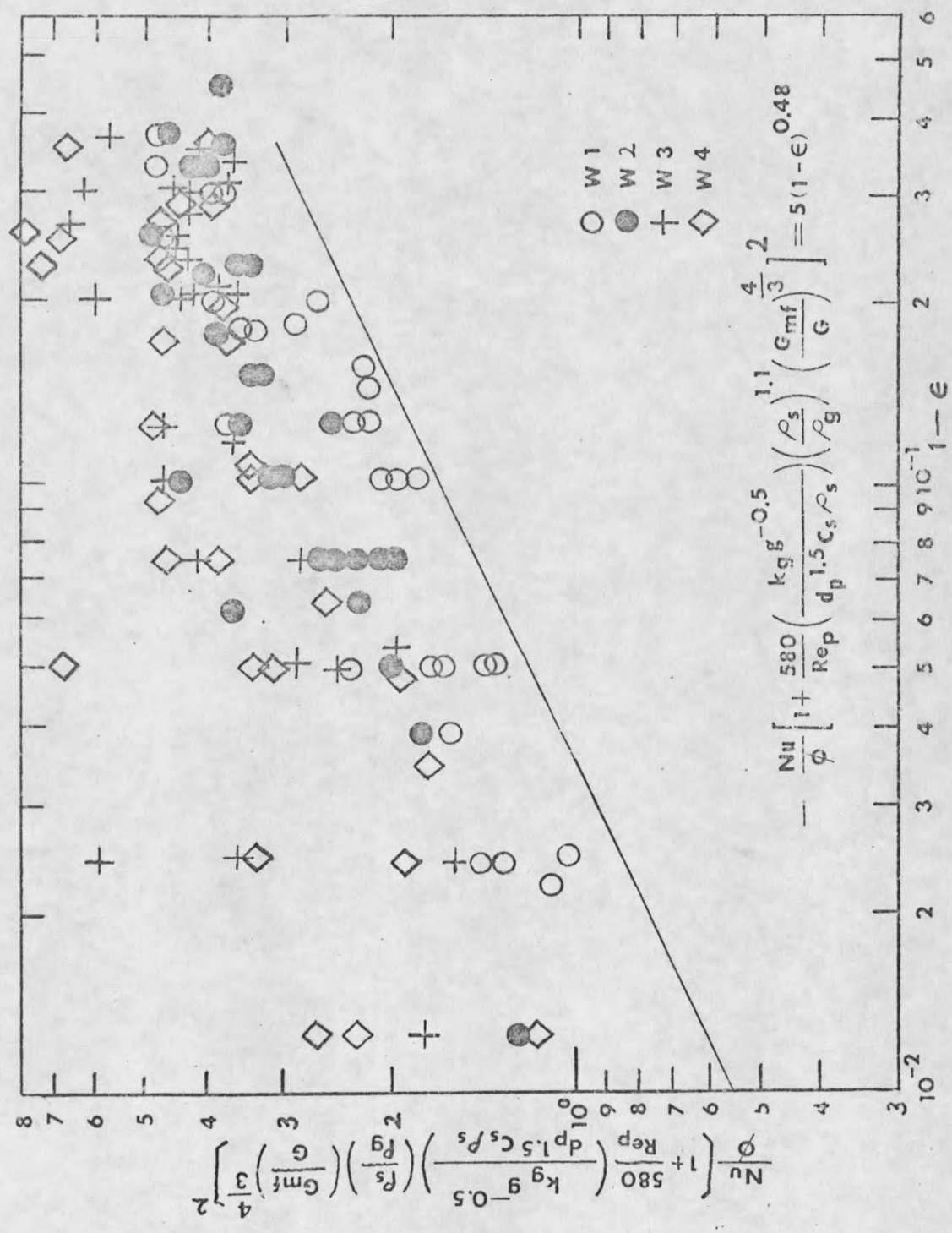


Figure 21. Average sectional coefficients.

The Modified Correlation According to The Sectional Coefficients

Equation 31 has been used to calculate average contact times, $\bar{\theta}$:

$$\bar{\theta} = \frac{\left(\sqrt{\frac{C_1(1-\epsilon)^{0.48}}{N_{up}}} - 1\right) \rho_s C_s d_p^2}{6k_g} \qquad (47)$$

With local Nusselt numbers and experimentally determined sectional particle fractions over the 11 different sections of the fluidized bed, average particle contact times, θ, were computed and the weighted averages of each run have been calculated with $C_1 = 10$.

Table III

The Weighted Average Contact Times

Amount of Extended Surfaces	$\frac{Y-1}{Y}$	$\bar{\theta}$, sec
w1, Y=6	0.83333	0.587
w2, Y=12	0.91667	0.483
w3, Y=18	0.94444	0.395
w4, Y=24	0.95833	0.376

Calculated weighted average contact times of static bed heights seven inches and nine inches are shown in Table III. As expected with the increasing amount of extended surfaces the average contact times were decreased. If the process of bed-of-wall heat transfer is visualized as the penetration of the boundary layer by quasi-fluid (particles ∿ gas) eddies from the bulk of the stream and the scouring action of the fluidized particles, then obviously the turbulence intensity would be expected to exert the most influence on the average contact time. That would be also true on the rate of heat transfer. The amount of extended surfaces, in other words turbulence promoters, have been increased from the value $\frac{Y-1}{Y}$ of 0.8333 to 0.91667, 0.94444 and to 0.95833. Particularly the size of eddies which would be expected to have some effect on the Nusselt number would exert some influence in the average contact time. Because the amount of boundary layer disruption and energy dissipation with the increase amount of extended surfaces (or turbulent promoters) are proportional to the eddy size.

Calculated contact times averaged 0.555 seconds for static bed height of 5 inches. These values are all in the range reported by Genetti (8) and Ziegler et al (34).

To obtain a correlation for the contact times,

θ, the dimensionless quantities $\frac{6k_g\tilde{\theta}}{\rho_s C_s D_p^2}$, $\frac{Y-1}{Y}$ and Re_p were calculated. These quantities are plotted on logarithm scales in Figure 22. The following correlation represents the data:

$$\frac{6k_g\tilde{\theta}}{\rho_s C_s D_p^2} = 6.856\ Re_p^{-1.1}\left(\frac{Y-1}{Y}\right)^{-0.8} \qquad (48)$$

By substituting θ, as expressed in Equation 48 into Equation 31, the following correlation for particle Nusselt numbers can be obtained with $C_1 = 10$:

$$Nu_p = \frac{10\ \phi(1-\varepsilon)^{0.48}}{\left[1 + \frac{6.856\ \left(\frac{Y-1}{Y}\right)^{-0.8}}{Re_p^{1.1}}\right]^2} \qquad (49)$$

where ϕ = spherity, the ratio of the surface area of the particle to the surface area of a sphere of same average diameter.

Y = number of tube diameter per 180° twist.

Microscopic enlargements of particles [Figure 7 (B)] shows that the glass particles used in this study are spherical, and $\phi = 1$ was used. Equation 49 as well as the experimental data, are shown in Figure 23. Static bed heights of five,

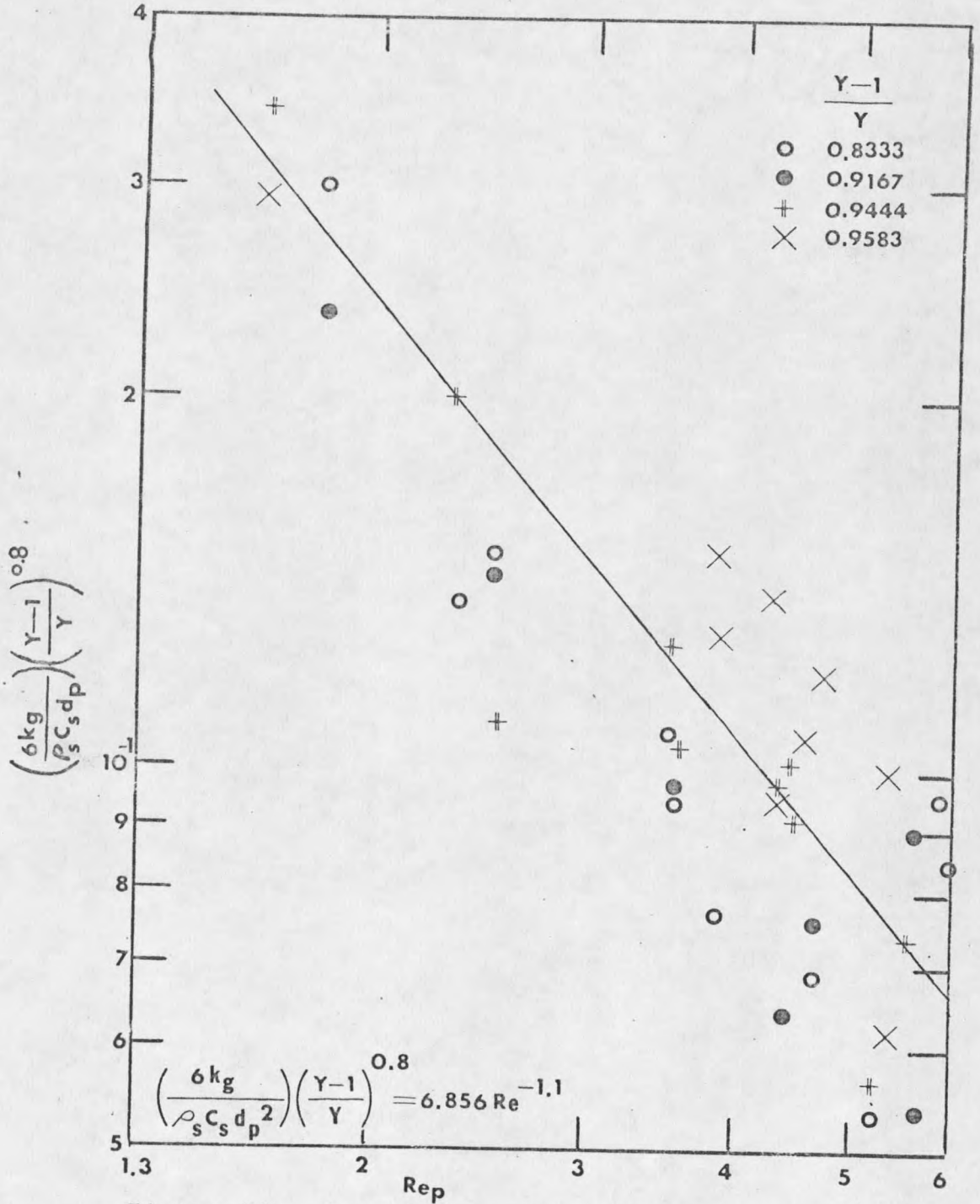


Figure 22. Correlation for average contact time.

seven, and nine inches are represented in the data shown in Figure 23. The values Y of 6, 12, 18, and 24 have been represented in the data shown in Figure 23. The modified correlation according to the sectional coefficients has been studied over 11 different points along the fluidized bed with different mass velocities. Most of the data (about 95 percent) are within $\pm$25 percent of Equation 49 in this study.

The exponent 0.48 for $1-\varepsilon$ cited by Genetti (8) with reference to other investigators (18, 20) agrees with the present investigation. Back-calculated weighted average contact times correlate with the present modified dimensionless groups and are in agreement with the previous calculations.

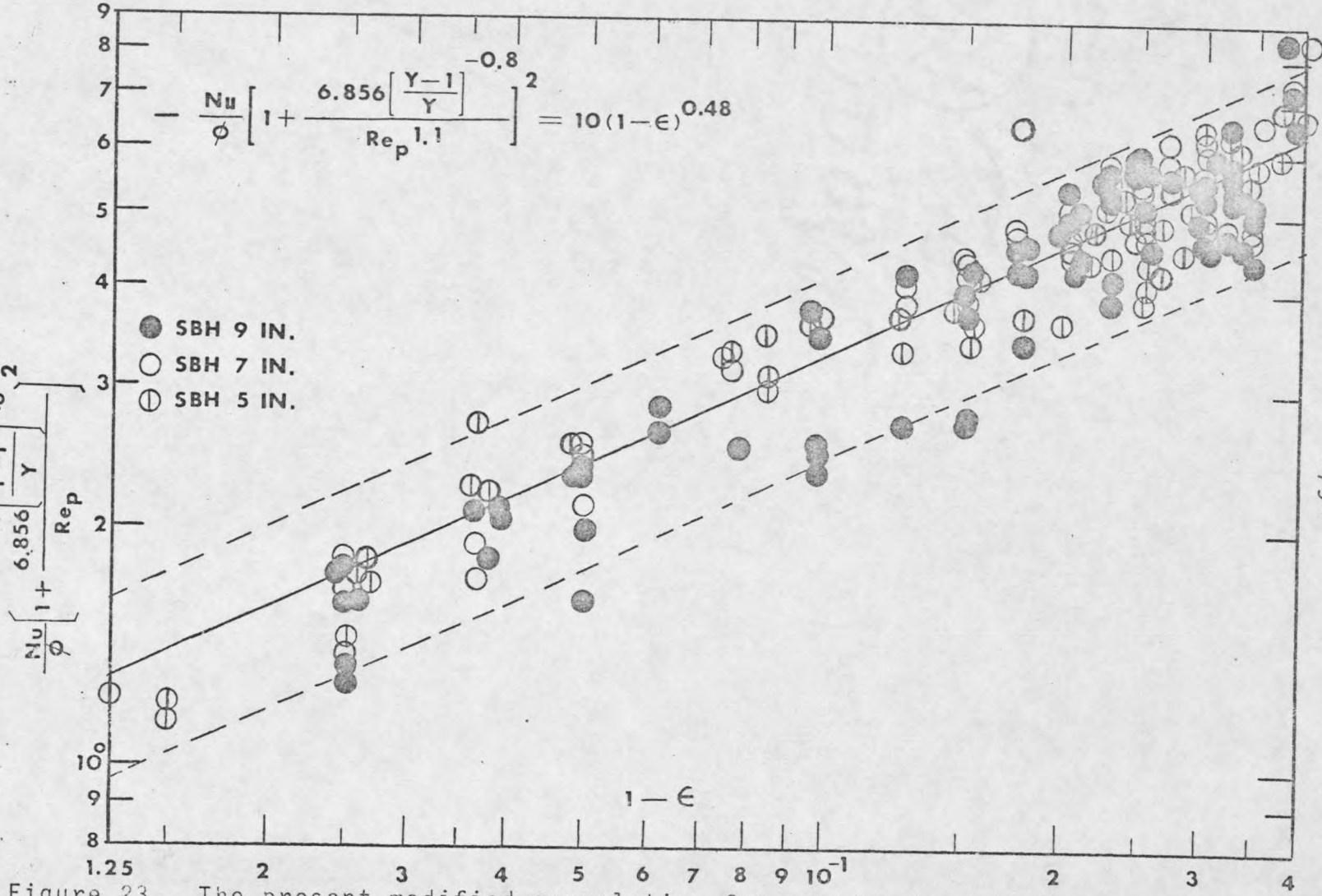


Figure 23. The present modified correlation for sectional particle Nusselt numbers.

Results and Conclusion

Local and average heat transfer coefficients for bed-to-wall heat transfer from a fluidized bed tubular heat exchanger with extended surfaces were investigated. Air was used as the fluidizing medium and coarse glass particles were fluidized in the experimental heat exchanger column. Heat transfer coefficients for air flowing through the heat exchanger without fluidization were also investigated.

Average Nusselt Numbers without Fluidization

The average heat transfer coefficients for air alone have been compared with those calculated from an accepted correlation form (6,8): it is concluded that higher coefficients were obtained in this study since extended surface area for heat transfer is available.

Fluidized Bed Thermal Gradients

From measurements of vertical fluidized bed temperature profiles, fluidized bed thermal gradients are shown to be very small. All profiles were showing uniformly distributed temperature profiles.

Local Heat Transfer Coefficients

Gradual increase in the weighted average heat transfer coefficients with respect to the number of extended surface

is observed throughout the runs. Local heat transfer coefficients are observed to decrease with the distance from the entrance of the fluidized bed. Local heat transfer coefficients varied slightly with different tube locations.

Average Sectional Coefficients

The average sectional coefficients have been compared with the data calculated from an established correlation (8). None of the data of this study is below Genetti's data for bare tubes. As expected, an increase in average sectional coefficients with respect to extended surface area is obtained. It is found that the exponent for $1-\varepsilon$ range from 0.46 to 0.52.

The Modified Correlation According to the Sectional Coefficients

With local heat transfer coefficients and experimentally determined sectional particle fractions over the 11 different sections of the fluidized bed, Nusselt numbers are correlated with Equation 49.

$$Nu_p = \frac{10\ \phi(1-\varepsilon)^{0.48}}{\left[1+\dfrac{6.856\ \left(\frac{\gamma-1}{\gamma}\right)^{-0.8}}{Re_p^{1.1}}\right]^2} \qquad (49)$$

Several conclusions can be drawn from this correlation:

1. Particle Nusselt numbers are dependent on twist ratio, Y. This also implies that particle Nusselt number is dependent upon extended surface area.

2. Particle Nusselt numbers are proportional to $(1-\varepsilon)^{0.48}$.

3. Particle Nusselt numbers have weak dependency on gas mass velocities.

Most of the data according to the modified correlation in this investigation are within $\pm$25 percent of Equation 49.

Literature Cited

1. Anderson, T.B. and Jackson, Roy, Ind. Eng. Chem. Fund., 6, 527 (1969).

2. Botterill, J.S.M. and Williams, J.R., Trans. Inst. Chem. Engrs., 41, 217 (1963).

3. Davidson, J.F., Trans. Inst. Chem. Engrs., 39, 230 (1961).

4. Davidson, J.F., Harrison, D., "Fluidized Particles," Cambridge University Press, New York (1963).

5. Dow, W.M. and Jakob, M., Chem. Eng. Prog., 47, 537 (1951).

6. Donohue, D.A., Ind. Eng. Chem., 41, 2499 (1949).

7. Frantz F. J., I. Chem. Eng., 69, 161 (Sept, 17,1962)
II. Ibid., page 89 (Oct. 1, 1962)
III. Ibid., page 103 (Oct. 29, 1962).

8. Genetti, W.E., Ph.D. Thesis, 1968, Oregon State University.

9. Gel'perin, N.I., Ainshtein, V.G. and Korotyanskaya, L.A., Int. Chem. Eng., 9, 137 (1969).

10. van Heerden, C., Nobel, P. and van Krevelen, D.W., Chem. Eng. Sci., 1, 51 (1951).

11. Kunii, D. and Levenspiel, O., Ind. Eng. Chem. Fund., 7, 446 (1968).

12. Kunii, D. and Levenspiel, O., Ind. Eng. Chem. Process Design and Development, 7, 481 (1968).

13. Kretzschmer, F., Forshung., Vol. 4, March-April, 1933, pages 93-95.

14. Kidd, G.J., Jr., A.I.Ch. E.J., 4, 581 (1969).

15. Leva, M., Weinstraub, M. and Grummer, M., Chem. Eng. Prog., 45, 563 (1949).

16. Levenspiel, O. and Walton, J.S., Chem. Eng. Prog. Symp. Ser., No. 9, Vol. 50, "Heat Transfer-Research Studies for 1954," A.L. Ch. E., pgs. 1-13.

17. Murray, J.D., J. Fluid Mech., 21, 465 (1965).

18. Mickley, H.S. and Fairbanks, D.F., A. I. Ch. E. J., 1, 374 (1955).

19. McAdams, W.H., "Heat Transmission," 3rd, ed., New York, McGraw-Hill, 1954, page 299.

20. Mickley, H.S. and Trilling, C.A., Ind. Eng. Chem., 41, 1135 (1949).

21. Miller, C. O. and Logwinuk, A. K., Ind. Eng. Chem., 43 1220 (1951).

22. Noe, A.R. and Knudsen, J.G., Chem. Eng. Prog. Symp. Ser., Vol. 64, No. 82, "Heat Transfer," A. I. Ch. E., 1968, 202-211.

23. Petrie, J. C., Freeby, W. A. and J. A., Chem. Eng. Prog., 64, 45 (1968).

24. Ruckenstein, E., Proceedings of the Third International Heat Transfer Conference, Papers 113-151, Vol. IV, page 298-301 (1966).

25. Szekely, J. and Fisher, R. J., Chem. Eng. Sci., 24, 833 (1969).

26. Toor, H. L. and Marchello, J. M., A. I. Ch. E. J., 4, 97, (1958).

27. Toomey, R.D. and Johnstone, H.F., Chem. Eng. Prog. Symp. Ser., Vol. 49, No. 5, "Heat Transfer," A. I. Ch. E., 1953, pages 51-63.

28. Vreedenbert, H.A., J. Appl. Chem., 2, 526 (1952).

29. Vreedenberg, H.A., Chem. Eng. Sci., 11, 274 (1960).

30. Wender, L. and Cooper, G.T., A. I. Ch. E. J., 4, 15 (1958).

31. Wen, C. Y. and Leva, M., A. I. Ch. E. J., 2, 482 (1956).

32. Wicke, E. and Fetting, F., Chemie-Ingr. Tech., 26, 301 (1954.

33. Yoshida, K., Kunii, D. and Levenspiel, O., Int. J. Heat Mass Transfer, 12, 529 (1969).

34. Ziegler, E. N., Koppel, L. B. and Brazelton, W. T., Ind. Eng. Chem. Fund., 3, 224 (1964).

Appendix I

Nomenclature

Symbol	Definition	Dimensions
A'	A very small constant for Equation 18	Dimensionless
A	Total surface area of particles in the bed	ft^2
A_h	Crossectional area of heat exchanger	ft^2
A_m	Cross-section area of a flow meter	ft^2
A_o	Cross-sectional area of orifice opening	ft^2
A_p	Surface area of particle/unit length of bed	ft^2 /ft
A_T	Surface area of entire solid bed	ft^2
a	coefficient for Equation 32	Dimensionless
b	Coefficient for Equation 32	Dimensionless
B'	A constant which increases with particle size for Equation 18	Dimensionless
C	Coefficient of discharge	Dimensionless
C_o	Constant	Dimensionless
C_1	Constant	Dimensionless
C_2	Constant	Dimensionless
C_g	Specific heat of gas	$Btu/lb_m°F$
C_{pg}	Specific heat of gas at constant pressure	$Btu/lb_m°F$
C_{ps}	Specific heat of solid at constant pressure	$Btu/lb_m°F$
C_R	Correction for non-axial tube location, for case of internal heat transfer surface	Dimensionless
C_s	Specific heat of solid	$But/lb_m°F$
D_1	Outer diameter of axial cylinder	ft

D_2	Daimeter of fluidized bed	ft
d_b	Effective diameter of bubble	ft
d_p, D_p	Particle diameter	ft
D_t	Tube diameter	ft
d_{ti}	Outer diameter of horizontal immersed tube	ft
emf	Electromotive force produced by the thermocouple	milivolts
F	Term defined in Equation 14	Dimensionless
g	Acceleration due to gravity	ft/hr^2
g_c	Gravitational Constant	$\frac{lb_m ft}{lb_f sec^2}$
G	Gas mass velocity	$lb_m/hr\ ft^2$
G_f	Mass velocity of fluidization of a bed	$lb_m/hr\ ft^2$
G_{mf}	Calculated minimum fluidizing gas mass velocity	$lb_m/hr\ ft^2$
h	Heat transfer coefficient	Btu/hr ft°F
h_{av}	Average heat transfer coefficient	Btu/hr ft°F
h_{loc}	Local heat transfer coefficient	$Btu/ft^2°F$
h_t	Time-averaged heat transfer coefficient	$Btu/ft^2°F$
h_{ti}	Local instantaneous heat transfer coefficient	$Btu/ft^2°F$
h_w	Heat transfer coefficient between bed and surface	$Btu/ft^2°F$
Δh	Manometer readings	ft
I(t)	Age distribution function of emulsion elements on the surface	Dimensionless
I	Current flowing through the heating element	Amperes

K	Kretzchmer coefficient	
k	Thermal conductivity	Btu/hr ft°F
k_e	Effective thermal conductivity of emulsion layer	Btu/ ft°f
k_g	Thermal conductivity of gas	Btu/ft hr°F
k_s	Thermal conductivity of solid	But/ft hr°F
l_e	Effective thickness of emulsion layer	ft
L	Bed height	ft
L_f	Mean height of fluidized bed	ft
L_h	Length of heat transfer surface	ft
L_{mf}	Height of bed at minimum fluidizing conditions	ft
L_s	Bed settled height	ft
M	Term defined in Equation 20	Dimensionless
N_{up}	Particle Nusslet number hD_p/k_g	Dimensionless
N_{uav}	Average particle Nusslet number, $h_{av}D_p/k_g$	Dimensionless
P	Pressure	lb_f/ft^2
P_1	Upstream pressure	lb_f/ft^2
P_2	Downstream pressure	lb_f/ft^2
ΔP_o	Orifice pressure drop	lb_f/ft^2
P_r	Prandtl number $C_g\mu/k_g$	Dimensionless
Q	Heat flux from heat transfer surface	Btu/hr ft^2
q_l	Rate of heat loss from fluidized bed	Btu/hr
R	Bed expansion ratio	Dimensionless

q_p	Heat transfer to a particle near the heat transfer surface	But/hr ft^2
R_e	Reynolds number	Dimensionless
R_{ep}	Particle Reynolds number, $D_p G/\mu$	Dimensionless
r	Radial distance from the center of the bed	ft
T	Temperature	°F
T_1, T_2	Inlet and outlet temperature respectively	°F
T_b	Bed temperature	°F
T_g	Average temperature of gas at any level in bed	°F
T_{gb}, T_{ge}	Temperature of bubble gas, and of emulsion gas	°F
T_{gi}	Inlet gas temperature	°F
T_{go}	Initial gas temperature	°F
T_s	Solid temperature	°F
T_w	Wall temperature	°F
u_b, u_{br}	Rising velocity of a bubble in a bubbling bed and velocity of bubble with respect to emulsion ahead of it	ft/hr
u_e	Upward gas velocity within emulsion phase	ft/hr
u_f	u_{mf}/ε_{mf}	ft/hr
u_{mf}	Superficial gas velocity at minimum fluidization conditions	ft/hr
u_o	Superficial gas velocity (based on empty tube)	ft/hr
u_s	Downward velocity of solids in emulsion phase	ft/hr
V	Voltage drop across the heating element	volts

v	Volumetric flow rate	ft^3/hr
v_f, v_g	Velocity of gas	ft/hr
$\dot{w}$	Actual mass flow rate	———
w_g	Gas flow rate	lb_m/hr
w_s	Superficial velocity of gas	ft/hr
x	Film thickness or distance from the heat exchange surface	ft
w_c	Gas flow rate times specific heat of gas	$\frac{BTU}{°F\ hr}$
Y	Expansion factor	Dimensionless
Y	Term defined in Equation 13	Dimensionless
Y	Twist ratio; the number of tube diameter per 180° twist	Dimensionless
Z	Term defined in Equation 15	Dimensionless

Volumetric Fraction of Solids

Symbol	Definition	Dimensions
α	Volume of emulsion transported upwards behing a bubble per volume of a bubble	Dimensionless
β	Ratio of the orifice diameter to the pipe diameter	Dimensionless
γ	Volumetric fraction of solids	Dimensionless
γ_p	Number of particles per unit surface area	particles/ft^2
ε	Void fraction	Dimensionless
ε_e	Void fraction of emulsion phase	Dimensionless
ε_f	Average void fraction in the fluidized bed	Dimensionless
ε_m	Void fraction of static bed	Dimensionless
ε_{mf}	Void fraction of bed at minimum fluidization conditions	Dimensionless
η	Fluidization efficiency, or $\frac{T_2-T_s}{T_1-T_s}$	Dimensionless
θ	Contact time	hr
$\bar{\theta}$	Average contact time	hr
ρ_b	Bed density	lb_m/ft^3
ρ_e	Apparent density of emulsion	lb_m/ft^3
ρ_g	Gas density	lb_m/ft^3
ρ_{gi}	Gas density of upstream location	lb_m/ft^3
ρ_s	Particle density	lb_m/ft^3
μ	Viscosity	$lb_m/ft\ hr$
μ_g	Gas viscosity	$lb_m/ft\ hr$

ν	Kinematic viscosity	ft^2/hr
ϕ_s	Sphericity	Dimensionless
ϕ	Ratio of the particle surface area to the area of a spherical particle of the same diameter	Dimensionless
δ	Volume fraction of bubbles in fluidized bed	Dimensionless

Appendix II

Evaluation of η and R

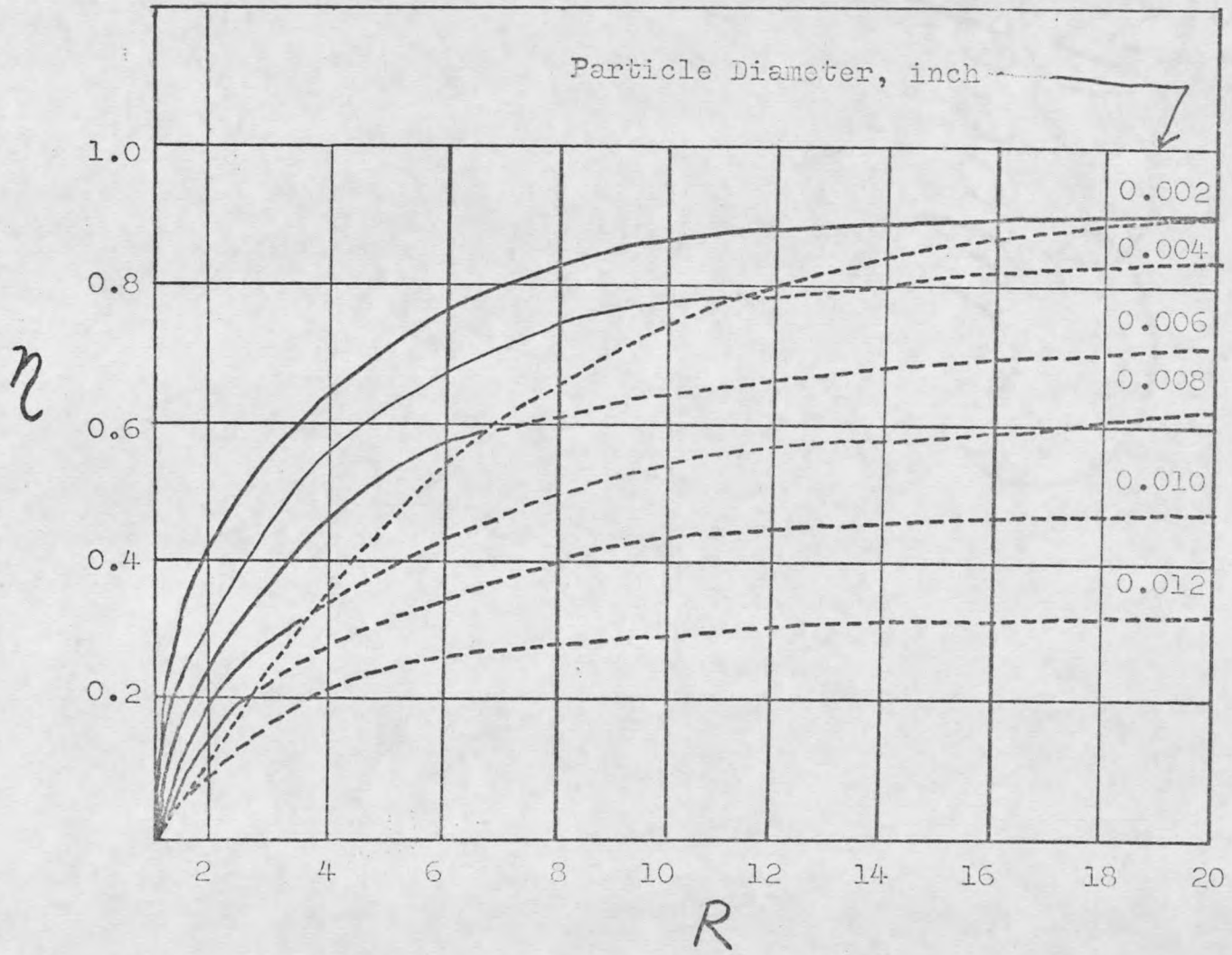


Figure 24. The correlation for η and R.

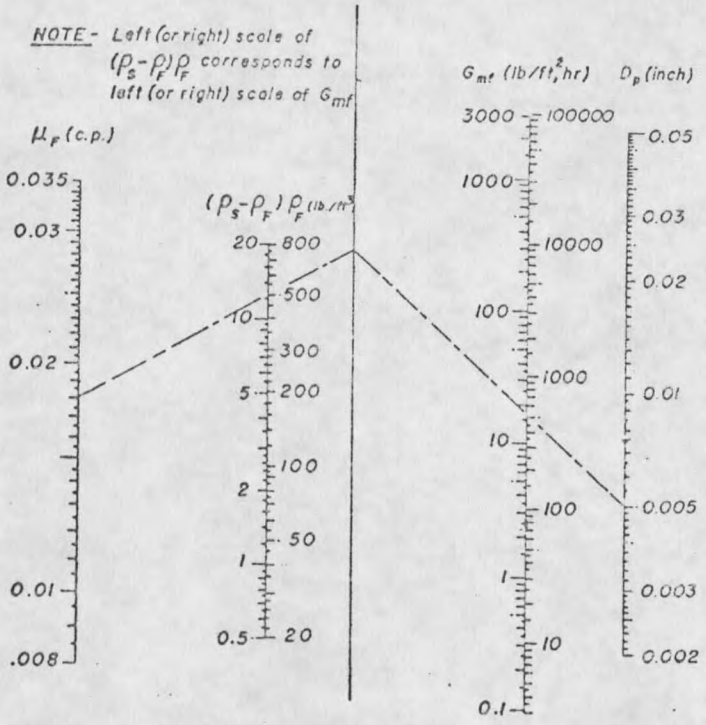


Figure 25. Nomograph to calculate G_{mf}.

Appendix III

A typical data sheet

Sample Raw Data Sheet

Run: 9H3W3 June 2, 1969

Time Started: 10:25 A.M.
Time Finished: 2.45 P.M.

Number of Exended Surfaces: 3

Static Bed Height: 9 inches
Fluidized Bed Height: 38 inches

Voltmeter Readings: 7.5 volts, 7.7 volts

Ammeter Readings: 50 amps 51 amps

Manometer (1) reading: (22 3/8 ∿ 22 1/4 inch)
(21 3/8 ∿ 21 1/4 inch) (for air flow rate)

Tube Wall Probe Thermocouples
emf by mv

	Location 1	Location 2	Location 3	Location 4
Probe 1	2.319	2.549	2.458	2.380
Probe 2	2.077	2.332	2.273	2.197
Probe 3	1.853	2.018	2.018	1.975
Probe 4	1.740	1.797	1.815	1.791
Prove 5	1.587	1.637	1.695	1.671
Probe 6	1.552	1.570	1.587	1.588
Probe 7	1.549	1.559	1.575	1.569
Probe 8	1.543	1.541	1.568	1.559
Probe 9	1.551	1.557	1.575	1.557
Probe 10	1.571	1.566	1.563	1.542
Probe 11	1.598	1.574	1.557	1.542

Bulk Bed Thermocouples
emf by mv

Section 1	1.815	Section 7	1.825
Section 2	1.838	Section 8	1.804
Section 3	1.837	Section 9	1.809
Section 4	1.834	Section 10	1.807
Section 5	1.825	Section 11	1.815
Section 6	1.825		

Manometer (2) Reading, Inches

Manometer 1	Δh	3.25
Manometer 2	Δh	3.00
Manometer 3	Δh	2.25
Manometer 4	Δh	2.00
Manometer 5	Δh	1.25
Manometer 6	Δh	0.75
Manometer 7	Δh	0.50
Manometer 8	Δh	0.125
Manometer 9	Δh	0.00
Manometer 10	Δh	0.00
Manometer 11	Δh	4.00

Appendix IV

Calibration Tables for Thermocouples

Chromel-Alumel Thermocouples

°F	0	1	2	3	4	5	6	7	8	9
60	0.618	0.640	0.662	0.684	0.706	0.729	0.751	0.774	0.096	0.818
70	0.840	0.862	0.884	0.906	0.929	0.951	0.974	0.996	1.019	1.041
80	1.064	1.086	1.109	1.131	1.154	1.176	1.199	0.221	1.244	1.266
90	1.289	1.311	1.334	1.357	1.380	1.403	1.426	1.448	1.471	1.193
100	1.516	1.538	1.561	1.583	1.607	1.630	1.653	1.676	1.699	1.722
110	1.745	1.768	1.791	1.814	1.837	1.859	1.882	1.905	1.928	1.951
120	1.974	1.997	2.020	2.043	2.066	2.088	2.111	2.134	2.157	2.180
130	2.203	2.225	2.248	2.270	2.293	2.316	2.340	2.363	2.386	2.409
140	2.433	2.455	2.478	2.500	2.523	2.546	2.569	2.593	2.616	2.639
150	2.663	2.685	2.708	2.730	2.753	2.776	2.799	2.822	2.846	2.869
160	2.892	2.915	2.937	2.960	2.982	3.006	3.029	3.052	3.076	3.099
170	3.122	3.145	3.169	3.192	3.215	3.239	3.262	3.285	3.309	3.332
180	3.355	3.378	3.402	3.424	3.447	3.469	3.492	3.515	3.538	3.562
190	3.585	3.608	3.632	3.655	3.678	3.701	3.725	3.748	3.771	3.795
200	3.818	3.841	3.865	3.883	3.911	3.934	3.958	3.981	4.004	4.028

Iron Constantan Thermocouples

°F	0	1	2	3	4	5	6	7	8	9
60	0.785	0.813	0.842	0.871	0.900	0.929	0.957	0.986	1.015	1.044
70	1.073	1.101	1.30	1.159	1.188	1.217	1.246	1.274	1.303	1.332
80	1.361	1.389	1.418	1.447	1.476	1.505	1.533	1.562	1.591	1.620
90	1.649	1.678	1.797	1.736	1.765	1.794	1.823	1.852	1.881	1.910
100	1.939	1.968	1997	2.026	2.055	2.084	2.113	2.143	2.1722	2.201
110	2.230	2.259	2.289	2.318	2.347	2.376	2.405	2.435	2.464	2.493

Appendix V

Complete Data
(Table IV)

RUN NO. 5W1H1 FBH IN 9
G = 527 $lb_m/hr\ ft^2$, Re_p = 18.228

Probe no.	1 — ∈	h_{loc}, Btu/hr ft^2 °F
1	0.0	0.79
2	0.0	1.12
3	0.0	1.29
4	0.0	1.87
5	0.0	2.27
6	0.0	2.69
7	0.0	3.90
8	0.0	6.65
9	0.0	21.49
10	0.1	34.23
11	0.375	34.10

Q = 267 Btu/hr ft^2, h_{av} = 9.0 Btu/hr ft^2 °F

RUN NO. 5W1H2 FBH IN 16
G = 1009 $lb_m/hr\ ft^2$, Re_p = 34.9

Probe no.	1 — ∈	h_{loc}, Btu/hr ft^2 °F
1	0.0	3.05
2	0.0	3.29
3	0.0	3.49
4	0.0	3.78
5	0.0	4.51
6	0.0	6.20
7	0.0	11.09
8	0.00625	22.34
9	0.1	38.37
10	0.225	39.24
11	0.325	45.65

Q = 333 Btu/hr ft^2, h_{av} = 16.4 Btu/hr ft^2 °F

RUN NO. 5W1H3 FBH IN 5
$G = 1254$ $lb_m/hr\,ft^2$, $Re_p = 43.375$

Probe no.	$1-\epsilon$	h_{loc}, Btu/hr ft^2 °F
1	0.0	2.89
2	0.0	3.24
3	0.0	3.46
4	0.0	4.44
5	0.0	6.18
6	0.0625	8.71
7	0.0125	18.11
8	0.05	23.13
9	0.15	28.74
10	0.25	30.35
11	0.225	33.70

$Q = 301$ Btu/hr ft^2, $h_{av} = 14.3$ Btu/hr ft^2 °F

RUN NO. 5W1H4 FBH IN 38
$G = 1443$ $lb_m/hr\,ft^2$, $Re_p = 49.912$

Probe no.	$1-\epsilon$	h_{loc}, Btu/hr ft^2 °F
1	0.0	4.33
2	0.0	5.14
3	0.0	6.18
4	0.0	7.42
5	0.0125	10.12
6	0.025	14.87
7	0.0375	18.96
8	0.075	25.21
9	0.15	27.32
10	0.2	29.59
11	0.275	34.16

$Q = 316$ Btu/hr ft^2, $h_{av} = 16.3$ Btu/hr ft^2 °F

RUN NO. 5W2 FBH IN 8
G = 527 $lb_m/hr\,ft^2$, Re_p = 18.228

Probe no.	1 — ∈	h_{loc}, Btu/hr ft² °F
1	0.0	0.69
2	0.0	0.86
3	0.0	1.11
4	0.0	1.58
5	0.0	2.29
6	0.0	2.77
7	0.0	3.86
8	0.0	5.76
9	0.0	2.125
10	0.075	39.28
11	0.375	39.78

Q = 280 Btu/hr ft², h_{av} = 9.5 Btu/hr ft² °F

RUN NO. 5W2H2 FBH IN 14
G = 1009 $lb_m/hr\,ft^2$, Re_p = 34.9

Probe no.	1 — ∈	h_{loc}, Btu/hr ft² °F
1	0.0	2.60
2	0.0	2.83
3	0.0	3.12
4	0.0	3.48
5	0.0	5.86
6	0.0	7.63
7	0.0	11.28
8	0.0	25.01
9	0.1	38.85
10	0.225	41.23
11	0.325	44.52

Q = 294 Btu/hr ft², h_{av} = 16.1 Btu/hr ft² °F

RUN NO. 5W2H3 FBH IN 25
G = 1273 $lb_m/hr\,ft^2$, Re_p = 43.997

Probe no.	1 — ∈	h_{loc}, Btu/hr ft² °F
1	0.0	3.45
2	0.0	3.77
3	0.0	4.84
4	0.0	6.22
5	0.0	9.53
6	0.025	14.78
7	0.05	20.62
8	0.0875	26.48
9	0.125	38.38
10	0.2	38.67
11	0.275	45.16

Q = 285 Btu/hr ft², h_{av} = 18.6 Btu/hr ft² °F

RUN NO. 5W2H4 FBH IN 33
G = 1459 $lb_m/hr\,ft^2$, Re_p = 50.43

Probe no.	1 — ∈	h_{loc}, Btu/hr ft² °F
1	0.0	4.66
2	0.0	5.55
3	0.0	7.33
4	0.0	9.73
5	0.125	12.25
6	0.025	17.47
7	0.0375	19.51
8	0.0875	22.83
9	0.125	27.61
10	0.175	30.05
11	0.275	34.33

Q = 281 Btu/hr ft², h_{av} = 17.1 Btu/hr ft² °F

RUN NO. 5W3H1 FBH IN 9
G = 481 $lb_m/hr\,ft^2$, Re_p = 16.637

Probe no.	1 — ∈	h_{loc}, Btu/hr ft^2 °F
1	0.0	1.02
2	0.0	1.93
3	0.0	2.08
4	0.0	2.76
5	0.0	3.55
6	0.0	4.25
7	0.0	5.70
8	0.0	9.77
9	0.0125	32.60
10	0.125	41.71
11	0.35	32.11

Q = 261 Btu/hr ft^2, h_{av} = 11.6 Btu/hr ft^2 °F

RUN NO. 5W3H2 FBH IN 16
G = 1009 $lb_m/hr\,ft^2$, Re_p = 34.9

Probe no.	1 — ∈	h_{loc}, Btu/hr ft^2 °F
1	0.0	3.56
2	0.0	3.98
3	0.0	4.20
4	0.0	4.69
5	0.0	5.80
6	0.0	8.54
7	0.0	18.08
8	0.025	26.98
9	0.075	41.21
10	0.325	40.71
11	0.30	35.68

Q = 276 Btu/hr ft^2, h_{av} = 17 Btu/hr ft^2 °F

RUN NO. 5W3H3 FBH IN 25
G = 1273 $lb_m/hr\,ft^2$, Re_p = 43.997

Probe no.	1 — ∈	h_{loc}, Btu/hr ft^2 °F
1	0.0	4.35
2	0.0	4.86
3	0.0	5.70
4	0.0	7.42
5	0.00625	10.61
6	0.01875	16.38
7	0.025	20.44
8	0.075	24.93
9	0.125	31.16
10	0.175	34.27
11	0.25	34.55

Q = 276 Btu/hr ft^2, h_{av} = 17.3 Btu/hr ft^2 °F

RUN NO. 5W3H4 FBH IN 38
G = 1410 $lb_m/hr\,ft^2$, Re_p = 48.77

Probe no.	1 — ∈	h_{loc}, Btu/hr ft^2 °F
1	0.0	9.18
2	0.00625	9.62
3	0.0125	10.18
4	0.025	12.27
5	0.025	15.26
6	0.0125	19.19
7	0.0375	22.48
8	0.0875	24.37
9	0.1	29.16
10	0.175	31.84
11	0.25	20.95

Q = 269 Btu/hr ft^2, h_{av} = 19.2 Btu/hr ft^2 °F

RUN NO. 5W4H1 FBH IN 9
G = 481 $lb_m/hr\ ft^2$, Re_p = 16.637

Probe no.	1 — ∈	h_{loc}, Btu/hr ft^2 °F
1	0.0	1.78
2	0.0	2.10
3	0.0	2.46
4	0.0	3.04
5	0.0	3.38
6	0.0	4.04
7	0.0	5.51
8	0.0	9.42
9	0.00625	33.43
10	0.1	41.17
11	0.4	37.49

Q = 236 Btu/hr ft^2, h_{av} = 12 Btu/hr ft^2 °F

RUN NO. 5W4H2 FBH IN 16
G = 1032 $lb_m/hr\ ft^2$, Re_p = 35.661

Probe no.	1 — ∈	h_{loc}, Btu/hr ft^2 °F
1	0.0	3.58
2	0.0	4.02
3	0.0	4.40
4	0.0	5.27
5	0.0	6.20
6	0.0	8.82
7	0.0625	17.16
8	0.0375	25.63
9	0.1	33.47
10	0.2	30.99
11	0.3	24.91

Q = 232 Btu/hr ft^2, h_{av} = 14.7 Btu/hr ft^2 °F

RUN NO. 5W4H3 FBH IN 24
G = 1217 $lb_m/hr\,ft^2$, Re_p = 42.06

Probe no.	1 — ∈	h_{loc}, Btu/hr ft^2 °F
1	0.0	4.31
2	0.0	4.86
3	0.0	5.63
4	0.0	7.36
5	0.0	10.19
6	0.0125	15.40
7	0.025	21.91
8	0.0625	35.65
9	0.1	46.00
10	0.3	48.63
11	0.25	38.47

Q = 240 Btu/hr ft^2, h_{av} = 21.3 Btu/hr ft^2 °F

RUN NO. 5W4H4 FBH IN38
G = 1360 $lb_m/hr\,ft^2$, Re_p = 47.041

Probe no.	1 — ∈	h_{loc}, Btu/hr ft^2 °F
1	0.0	7.16
2	0.0	8.42
3	0.00625	10.37
4	0.0125	12.72
5	0.0125	16.25
6	0.025	20.12
7	0.05	23.79
8	0.0625	30.43
9	0.1	37.04
10	0.15	38.99
11	0.25	39.00

Q = 254 Btu/hr ft^2, h_{av} = 21.9 Btu/hr ft^2 °F

RUN NO. 7W1H1 FBH IN 12
G = 680 $lb_m/hr\,ft^2$, Re_p = 23.521

Probe no.	1 — ∈	h_{loc}, Btu/hr ft^2 °F
1	0.0	1.67
2	0.0	1.49
3	0.0	1.52
4	0.0	2.11
5	0.0	2.79
6	0.0	3.70
7	0.0	6.34
8	0.0	17.67
9	0.5	33.89
10	0.35	42.01
11	0.375	47.74

Q = 276 Btu/hr ft^2, h_{av} = 13.4 Btu/hr ft^2 °F

RUN NO. 7W1H2 FBH IN 22
G = 1097 $lb_m/hr\,ft^2$, Re_p = 37.91

Probe no.	1 — ∈	h_{loc}, Btu/hr ft^2 °F
1	0.0	2.94
2	0.0	3.21
3	0.0	3.53
4	0.0	4.91
5	0.0	7.56
6	0.0	14.96
7	0.025	30.94
8	0.125	40.16
9	0.25	41.12
10	0.25	40.46
11	0.275	46.91

Q = 292 Btu/hr ft^2, h_{av} = 21.1 Btu/hr ft^2 °F

RUN NO. 7W1H3 FBH IN 31
G = 1325 $lb_m/hr\,ft^2$, Re_p = 45.865

Probe no.	1 — ∈	h_{loc}, Btu/hr ft² °F
1	0.0	3.84
2	0.0	4.77
3	0.0	6.12
4	0.0	7.57
5	0.025	13.34
6	0.05	21.72
7	0.125	33.27
8	0.175	32.29
9	0.2	36.43
10	0.2	37.10
11	0.275	44.49

Q = 310 Btu/hr ft², h_{av} = 21.6 Btu/hr ft² °F

RUN NO. 7W1H4 FBH IN 40
G = 1490 $lb_m/hr\,ft^2$, Re_p = 51.538

Probe no.	1 — ∈	h_{loc}, Btu/hr ft² °F
1	0.0	6.54
2	0.00635	8.25
3	0.00635	9.85
4	0.0125	11.30
5	0.0375	14.55
6	0.05	21.63
7	0.05	32.54
8	0.125	37.72
9	0.125	43.52
10	0.175	43.91
11	0.225	58.40

Q = #@) Btu/hr ft², h_{av} = 25.6 Btu/hr ft² °F

RUN NO. 7W2H1 FBH IN 12
G = 680 $lb_m/hr\,ft^2$, Re_p = 23.521

Probe no.	1 — ∈	h_{loc}, Btu/hr ft^2 °F
1	0.0	2.43
2	0.0	2.63
3	0.0	2.99
4	0.0	3.52
5	0.0	4.47
6	0.0	6.04
7	0.0	10.42
8	0.0	28.94
9	0.0875	58.58
10	0.3	60.50
11	0.375	70.98

Q = 352 Btu/ hr ft^2, h_{av} = 21.1 Btu/hr ft^2 °F

RUN NO. 7W2H2 FBH IN 19
G = 1097 $lb_m/hr\,ft^2$, Re_p = 37.91

Probe no.	1 — ∈	h_{loc}, Btu/ hr ft^2 °F
1	0.0	2.90
2	0.0	3.25
3	0.0	3.60
4	0.0	4.35
5	0.0	5.63
6	0.0	8.49
7	0.0625	20.81
8	0.075	30.99
9	0.25	33.62
10	0.25	34.03
11	0.325	36.07

Q = 294 Btu/ hr ft^2, h_{av} = 16.2 Btu/hr ft^2 °F

RUN NO. 7W2H3 FBH IN 27
G = 1325 $lb_m/hr\,ft^2$, Re_p = 45.865

Probe no.	1 — ∈	h_{loc}, Btu/hr ft^2 °F
1	0.0	3.59
2	0.0	4.17
3	0.0	5.36
4	0.0	7.65
5	0.0	13.20
6	0.025	21.28
7	0.075	30.29
8	0.125	34.19
9	0.175	39.22
10	0.225	36.57
11	0.275	42.28

Q = 285 Btu/hr ft^2, h_{av} = 21.4 Btu/hr ft^2 °F

RUN NO. 7W2H4 FBH IN 38
G = 1490 $lb_m/hr\,ft^2$, Re_p = 51.538

Probe no.	1 — ∈	h_{loc}, Btu/hr ft^2 °F
1	0.0	4.58
2	0.0	5.54
3	0.00625	8.56
4	0.025	12.01
5	0.0375	16.56
6	0.05	26.12
7	0.0625	32.52
8	0.175	33.06
9	0.2	35.64
10	0.245	36.15
11	0.275	39.53

Q = 281 Btu/hr ft^2, h_{av} = 22.7 Btu/hr ft^2 °F

RUN NO. 7W3H1 FBH IN 15
G = 680 $lb_m/hr\,ft^2$, Re_p = 23.521

Probe no.	1 — ∈	h_{loc}, Btu/hr ft² °F
1	0.0	2.75
2	0.0	3.15
3	0.0	3.52
4	0.0	4.17
5	0.0	4.98
6	0.0	7.23
7	0.0	13.83
8	0.0	44.11
9	0.0625	47.65
10	0.175	45.55
11	0.3	37.11

Q = 255 Btu/hr ft², h_{av} = 18.9 Btu/hr ft² °F

RUN NO. 7W3H2 FBH IN 22
G = 1009 $lb_m/hr\,ft^2$, Re_p = 34.9

Probe no.	1 — ∈	h_{loc}, Btu/hr ft² °F
1	0.0	3.85
2	0.0	4.34
3	0.0	5.11
4	0.0	6.65
5	0.0	10.76
6	0.0	20.72
7	0.025	36.53
8	0.1	45.33
9	0.225	43.75
10	0.225	43.66
11	0.35	34.09

Q = 259 Btu/hr ft², h_{av} = 23.2 Btu/hr ft² °F

RUN NO. 7W3H3 FBH IN 31
G = 1238 $lb_m/hr\,ft^2$, Re_p = 42.821

Probe no.	1 — ∈	h_{loc}, Btu/hr ft^2 °F
1	0.0	4.88
2	0.0	5.88
3	0.0	7.83
4	0.00625	11.05
5	0.025	15.65
6	0.0375	23.76
7	0.075	35.12
8	0.15	37.61
9	0.2	40.43
10	0.25	36.77
11	0.35	36.99

Q = 268 Btu/hr ft^2, h_{av} = 23.3 Btu/hr ft^2 °F

RUN NO. 7W3H4 FBH IN 41
G = 1490 $lb_m/hr\,ft^2$, Re_p = 51.538

Probe no.	1 — ∈	h_{loc}, Btu/hr ft^2 °F
1	0.0	10.38
2	0.125	12.62
3	0.025	14.35
4	0.05	17.38
5	0.05	20.61
6	0.075	26.15
7	0.1	32.05
8	0.1	34.01
9	0.15	37.62
10	0.15	36.37
11	0.225	40.16

Q = 271 Btu/hr ft^2, h_{av} = 25.5 Btu/hr ft^2 °F

RUN NO. 7W4H1 FBH IN 15
G = 745 $lb_m/hr\,ft^2$, Re_p = 25.769

Probe no.	1 — ∈	h_{loc}, Btu/hr ft^2 °F
1	0.0	2.96
2	0.0	3.31
3	0.0	3.85
4	0.0	4.54
5	0.0	5.94
6	0.0	8.96
7	0.0	20.31
8	0.025	54.88
9	0.2	62.02
10	0.3	52.86
11	0.4	58.34

Q = 234 Btu/hr ft^2, h_{av} = 24.5 Btu/hr ft^2 °F

RUN NO. 7W4H2 FBH IN22
G = 1054 $lb_m/hr\,ft^2$, Re_p = 36.422

Probe no.	1 — ∈	h_{loc}, Btu/hr ft^2 °F
1	0.0	3.95
2	0.0	4.66
3	0.0	5.53
4	0.0	6.88
5	0.0	10.70
6	0.0125	21.41
7	0.0375	37.30
8	0.15	50.53
9	0.25	55.22
10	0.3	46.47
11	0.3	38.57

Q = 230, Btu/hr ft^2, h_{av} = 25.16 Btu/hr ft^2 °F

RUN NO. 7W4H3 FBH IN 31
G = 1235 $lb_m/hr\ ft^2$, Re_p = 42.717

Probe no.	1 — ∈	h_{loc}, Btu/hr ft^2 °F
1	0.0	5.03
2	0.0	6.37
3	0.0	8.33
4	0.00625	13.52
5	0.0125	17.10
6	0.05	26.33
7	0.1	39.20
8	0.125	40.37
9	0.2	45.23
10	0.2	38.92
11	0.3	36.75

Q = 249 Btu/hr ft^2, h_{av} = 25.4 Btu/hr ft^2 °F

RUN NO. 7W4H4 FBH IN 44
G = 1490 $lb_m/hr\ ft^2$, Re_p = 51.538

Probe no.	1 — ∈	h_{loc}, Btu/hr ft^2 °F
1	0.0	12.80
2	0.0	14.90
3	0.0	15.96
4	0.00625	18.96
5	0.0125	21.57
6	0.05	27.27
7	0.1	32.89
8	0.125	36.31
9	0.2	47.12
10	0.2	60.56
11	0.3	61.19

Q = 246 Btu/hr ft^2, h_{av} = 30.9 Btu/hr ft^2 °F

RUN NO. 9W1H1 FBH IN 21
G = 745 $lb_m/hr\,ft^2$, Re_p = 25.769

Probe no.	1 — ∈	h_{loc}, Btu/hr ft^2 °F
1	0.0	2.41
2	0.0	2.70
3	0.0	3.02
4	0.0	3.61
5	0.0	4.61
6	0.0	6.99
7	0.00625	18.54
8	0.15	29.33
9	0.3	36.34
10	0.3	37.69
11	0.375	47.20

Q = 271 Btu/hr ft^2, h_{av} = 16.7 Btu/hr ft^2 °F

RUN NO. 9W1H2 FBH IN 29
G = 745 $lb_m/hr\,ft^2$, Re_p = 34.9

Probe no.	1 — ∈	h_{loc}, Btu/hr ft^2 °F
1	0.0	3.48
2	0.0	4.35
3	0.0	5.52
4	0.0	8.53
5	0.025	14.406
6	0.05	24.094
7	0.125	36.119
8	0.175	31.99
9	0.2	37.21
10	0.3	36.91
11	0.325	47.58

Q = 292 Btu/hr ft^2, h_{av} = 22.5 Btu/hr ft^2 °F

RUN NO. 9W1H3 FBH IN 42
G = 745 $lb_m/hr\,ft^2$, Re_p = 50.431

Probe no.	1 — ∈	h_{loc}, Btu/hr ft^2 °F
1	0.0	8.98
2	0.025	9.87
3	0.025	11.53
4	0.05	12.79
5	0.05	15.23
6	0.1	17.54
7	0.1	18.89
8	0.15	21.92
9	0.2	23.95
10	0.25	26.96
11	0.35	34.43

Q = 279 Btu/hr ft^2, h_{av} = 18.1 Btu/hr ft^2 °F

RUN NO. 9W1H4 FBH IN 48
G = 887 $lb_m/hr\,ft^2$, Re_p = 57.625

Probe no.	1 — ∈	h_{loc}, Btu/hr ft^2 °F
1	0.0	11.09
2	0.025	13.34
3	0.025	13.29
4	0.0375	14.58
5	0.05	16.28
6	0.1	19.85
7	0.125	21.49
8	0.15	21.80
9	0.175	28.23
10	0.175	35.57
11	0.25	47.16

Q = 297 Btu/hr ft^2, h_{av} = 21.5 Btu/hr ft^2 °F

RUN NO. 9W2H1 FBH IN 17
G = 1009 $lb_m/hr\,ft^2$, Re_p = 25.769

Probe no.	1 − ∈	h_{loc}, Btu/hr ft^2 °F
1	0.0	3.50
2	0.0	4.37
3	0.0	4.82
4	0.0	5.88
5	0.0	7.23
6	0.0	12.39
7	0.0	21.14
8	0.0625	36.67
9	0.225	40.03
10	0.325	40.16
11	0.375	43.91

Q = 289 Btu/hr ft^2, h_{av} = 19.5 Btu/hr ft^2 °F

RUN NO. 9W2H2 FBH IN 24
G = 1054 $lb_m/hr\,ft^2$, Re_p = 36.42

Probe no.	1 − ∈	h_{loc}, Btu/hr ft^2 °F
1	0.0	4.95
2	0.0	6.03
3	0.0	6.90
4	0.0	10.57
5	0.0	14.74
6	0.0125	24.68
7	0.1	42.73
8	0.2	45.37
9	0.325	39.53
10	0.325	40.66
11	0.45	34.33

Q = 294 Btu/hr ft^2, h_{av} = 24.7 Btu/hr ft^2 °F

RUN NO. 9W2H3 FBH IN 38
$G = 1009$ $lb_m/hr\,ft^2$, $Re_p = 50.43$

Probe no.	$1-\epsilon$	h_{loc}, Btu/hr ft^2 °F
1	0.0	6.11
2	0.0	8.71
3	0.0125	12.35
4	0.0375	17.43
5	0.0625	21.59
6	0.1	31.95
7	0.15	32.49
8	0.15	31.47
9	0.225	32.03
10	0.225	33.18
11	0.35	36.67

$Q = 291$ Btu/hr ft^2, $h_{av} = 24.2$ Btu/hr ft^2 °F

RUN NO. 9W2H4 FBH IN 47
$G = 1054$ $lb_m/hr\,ft^2$, $Re_p = 57.62$

Probe no.	$1-\epsilon$	h_{loc}, Btu/hr ft^2 °F
1	0.0	15.75
2	0.0375	18.34
3	0.05	20.43
4	0.075	21.06
5	0.075	23.54
6	0.075	27.96
7	0.075	28.07
8	1.0	29.87
9	0.125	34.94
10	0.175	38.67
11	0.25	48.32

$Q = 355$ Btu/hr ft^2, $h_{av} = 27.6$ Btu/hr ft^2 °F

RUN NO. 9W4H1 FBH IN 21
$G_{}$ = 1666 $lb_m/hr\,ft^2$, Re_p = 30.68

Probe no.	1 − ∈	h_{loc}, Btu/hr ft^2 °F
1	0.0	3.77
2	0.0	4.50
3	0.0	5.36
4	0.0	7.07
5	0.0	13.06
6	0.0125	28.97
7	0.05	76.98
8	0.225	77.58
9	0.25	81.13
10	0.25	66.91
11	0.35	66.19

Q = 244 Btu/hr ft^2, h_{av} = 39.2 Btu/hr ft^2 °F

RUN NO. 9W4H2 FBH IN 27
G = 1694 $lb_m/hr\,ft^2$, Re_p = 36.422

Probe no.	1 − ∈	h_{loc}, Btu/hr ft^2 °F
1	0.0	4.78
2	0.0	5.31
3	0.0	7.90
4	0.00625	12.73
5	0.0125	21.66
6	0.05	36.15
7	0.125	46.49
8	0.225	43.45
9	0.25	45.07
10	0.35	38.82
11	0.35	34.95

Q = 246 Btu/hr ft^2, h_{av} = 27.5 Btu/hr ft^2 °F

RUN NO. 9W4H3 FBH IN 38
G = 1638 $lb_m/hr\,ft^2$, Re_p = 43.375

Probe no.	1 — ∈	h_{loc}, Btu/hr ft² °F
1	0.0	
2	0.00625	
3	0.0125	
4	0.025	
5	0.05	
6	0.075	
7	0.075	
8	0.175	
9	0.25	
10	0.25	
11	0.3	

Q = 246 Btu/hr ft², h_{av} = 31.6 Btu/hr ft² °F

RUN NO. 9W4H4 FBH IN 47
G = 1506 $lb_m/hr\,ft^2$, Re_p = 52.056

Probe no.	1 — ∈	h_{loc}, Btu/hr ft² °F
1	0.0	15.19
2	0.0375	17.97
3	0.05	20.42
4	0.0625	24.61
5	0.1	27.23
6	0.1	34.97
7	0.1	36.15
8	0.175	35.65
9	0.2	36.17
10	0.3	36.62
11	0.25	35.75

Q = 249 Btu/hr ft², h_{av} = 30.4 Btu/hr ft² °F

MONTANA STATE UNIVERSITY LIBRARIES
3 1762 10014638 8

N378
K562
cop.2

Kim, Joon Taik
Heat transfer in the finned fluidized bed tubular h[redacted]at exchanger

NAME AND ADDRESS

N378
K562
cop. 2